Environmental Science & Technology

pubs.acs.org/est

Article

Structure-Dependent Oxidation Mechanisms of Glyphosate by Manganese Oxides: Role of Mineralogy and pH

Zhe Liu, Mengqi Zhang, Ziyang Zhou, Xinyu Liu, Bruno Lanson, Wantong Zhao, Xionghan Feng, Wenfeng Tan, Guining Lu, and Xiaoming Wang*

Cite This: *Environ. Sci. Technol.* 2026, 60, 25686−25700

Read Online

ACCESS | Metrics & More | Article Recommendations | Supporting Information

ABSTRACT: The environmental persistence of glyphosate and its transformation into aminomethylphosphonic acid (AMPA) necessitate a mechanistic understanding of its abiotic degradation in natural environments. Manganese (Mn) oxides are ubiquitous redox-active minerals capable of oxidizing glyphosate; however, how Mn oxide mineralogy and pH regulate degradation kinetics, pathway selectivity, and interfacial redox processes remains unclear. Here, we investigated glyphosate oxidation by three representative Mn oxides, layered birnessite, disordered-layered vernadite, and tunnel-structured cryptomelane, across pH 3−7. Vernadite exhibited the highest and most sustained oxidative reactivity, cryptomelane showed rapid but strongly pH-dependent oxidation, and birnessite displayed slower yet persistent reactivity. Mineral structure controlled product selectivity: under near-neutral conditions, layered Mn oxides favored glycine formation through C−N bond cleavage adjacent to the phosphonate group, whereas tunnel-structured cryptomelane promoted AMPA accumulation through cleavage near the carboxyl group. Acidic conditions (pH 3 and 5) enhanced AMPA accumulation across all Mn oxides, suggesting increased persistence risks. Spectroscopic and kinetic analyses demonstrated that glyphosate oxidation involved surface complexation with Mn(IV), interfacial electron transfer, and propagation through transient, labile Mn(III) intermediates. These findings reveal that Mn oxide mineralogy and pH jointly govern bond-selective glyphosate oxidation and AMPA accumulation, advancing mechanistic predictions of glyphosate fate in soil and aquatic environments.

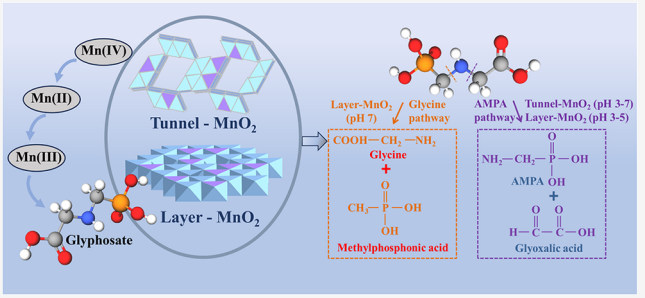

KEYWORDS: *manganese oxides, glyphosate, structure-dependent oxidation, degradation pathways, pH effects, AMPA formation, Mn redox cycling*

1. INTRODUCTION

Glyphosate [N-(phosphonomethyl)glycine] is the most widely used phosphonate herbicide worldwide,[1] with annual consumption estimated at 10^5−10^6 t.[2,3] Because of its limited uptake by target plants, a substantial fraction of applied glyphosate remains in agricultural soils through interactions with mineral surfaces, together with its primary metabolite aminomethylphosphonic acid (AMPA), which is more persistent and potentially more toxic than glyphosate.[4] These residues can be transported to aquatic systems via surface runoff and erosion in both dissolved and particulate forms.[5,6] The accumulation of glyphosate and AMPA poses ecotoxicological risks to nontarget organisms and has raised substantial public health concerns,[7] particularly after glyphosate was classified as a probable human carcinogen by the World Health Organization in 2015.[8] Therefore, elucidating the degradation mechanisms of glyphosate is essential for accurate ecological risk assessment and the development of effective remediation strategies.

The molecular structure of glyphosate ($C_3H_8NO_5P$), which contains phosphonate, amine, and carboxyl groups, enables multiple degradation pathways through both biotic and abiotic processes.[9] Reported transformation pathways include cleavage of the C(2)-N bond adjacent to the carboxyl group (AMPA pathway), cleavage of the C(3)-P bond (sarcosine pathway), and cleavage of the C(3)-N bond near the phosphonate group (glycine pathway).[10−12] Among naturally occurring abiotic oxidants in soils and sediments, manganese (Mn) oxides are particularly important because of their large specific surface area (SSA), low point of zero charge (PZC), and strong adsorption and oxidative capacities.[13−15] These properties make Mn oxides effective heterogeneous oxidants for a wide range of organic pollutants including pesticides, antibiotics, and phenolic compounds.[16−18]

Received: January 16, 2026
Revised: July 18, 2026
Accepted: July 20, 2026
Published: July 29, 2026

Previous studies have shown that Mn oxides, including birnessite (δ-MnO_2) and pyrolusite (β-MnO_2), can rapidly oxidize glyphosate, and that the degradation rate is strongly influenced by pH, temperature, and coexisting ions or organic molecules.[4,19−22] Specifically, carbonate, phosphate, humic acids, proteins, and Cu^{2+} inhibit glyphosate degradation by competing for surface adsorption sites or forming stable ternary complexes,[19,20,22] whereas lower pH and higher temperature enhance degradation by promoting glyphosate adsorption.[19,21] These studies further indicate that AMPA and glycine are the primary transformation products of glyphosate on birnessite, with their relative proportions determined by the glyphosate-to-birnessite ratio, reaction temperature, pH, protein coexistence, and adsorption configuration. For example, elevated temperature favors glycine formation,[21] while the presence of proteins promotes the AMPA pathway, particularly under acidic conditions, by facilitating monodentate mononuclear adsorption of the phosphonate group.[22] Birnessite may also mediate glyphosate degradation through the sarcosine pathway, although the rapid transformation of sarcosine likely prevents its detection.[20,22] Importantly, although the degradation pathways of glyphosate on birnessite have been extensively studied, the influence of Mn oxide mineralogy on these pathways remains unclear. This knowledge gap limits our ability to predict glyphosate fate across diverse soil and sediment systems.

Mechanistic studies suggest that glyphosate oxidation by birnessite is initiated by surface complexation between glyphosate functional groups and Mn(IV)−OH sites, which facilitates interfacial electron transfer from the nitrogen center to Mn(IV), ultimately leading to C−N bond cleavage.[12] Glyphosate oxidation at the birnessite interface may also proceed via direct single-electron transfer coupled with nucleophilic attack, resulting in bond cleavage at different positions within the molecule and the concomitant reduction of Mn(IV).[20,22] Previous studies further indicate that reactive oxygen species (ROS) can be generated under UV irradiation and contribute to bond cleavage,[23] whereas under dark conditions, ROS appear to play only a minor role.[20,22] In addition, soluble Mn(III) species have been shown to significantly influence the degradation of organic pollutants by birnessite.[24] However, the relative contributions of ROS generation, Mn(III)-mediated redox cycling, and direct interfacial electron transfer during Mn-oxide-mediated glyphosate oxidation remain unresolved. Moreover, whether these mechanisms vary systematically with the Mn oxide crystal structure and mineralogy has not yet been established.

Naturally occurring Mn oxides can be broadly classified into layered and tunneled-structural phases, which exhibit distinct crystal structures, surface properties, and redox behaviors.[25] Layered Mn oxides (δ-MnO_2), such as birnessite and vernadite, consist of two-dimensional sheets of edge-sharing [MnO_6] octahedra. δ-MnO_2 is among the most abundant Mn oxides in soils and sediments and serves as an important redox-active component in biogeochemical cycles.[13] Compared with birnessite, vernadite typically displays lower crystallinity, smaller particle size, and a higher degree of structural disorder, which collectively enhance its surface reactivity toward elemental cycling and contaminant transformation.[26,27] With long-term aging, layered Mn oxides can transform into tunnel-structured minerals such as cryptomelane (α-MnO_2).[28] Cryptomelane, widely distributed in soils and sediments, possesses a 2 × 2 tunnel framework and exhibits high adsorption capacity and strong oxidative potential, rendering it highly reactive toward organic contaminants.[29] These structural variations are expected to influence glyphosate reactivity on Mn oxide surfaces.[19] In addition, solution pH fundamentally governs Mn oxide surface charge, redox thermodynamics, and the aqueous speciation of glyphosate, thereby exerting coupled influences on degradation kinetics and transformation pathways.[19,22,30] Despite these advances, the combined influence of Mn oxide mineralogy and solution pH on glyphosate degradation remains poorly understood.

The objective of this study was to systematically elucidate the coupled effects of Mn oxide mineralogy and solution pH on the kinetics, transformation pathways, and underlying mechanisms of glyphosate degradation. Three representative Mn oxides, layered birnessite, disordered layered vernadite, and tunnel-structured cryptomelane, were selected to explicitly probe structure-dependent reactivity. Glyphosate degradation was examined over pH 3−7 using an integrated experimental approach that combined macroscopic kinetic measurements with molecular-scale spectroscopic analyses, including phosphorus (P) K-edge X-ray absorption near-edge structure (XANES) spectroscopy, X-ray photoelectron spectroscopy (XPS), ultraviolet−visible (UV−vis) spectroscopy, and electron paramagnetic resonance (EPR) spectroscopy. This study establishes a comprehensive mechanistic framework for abiotic glyphosate degradation by Mn oxides and highlights the critical roles of the mineral structure and pH in controlling glyphosate transformation and AMPA formation in soil and aquatic environments.

2. MATERIALS AND METHODS

2.1. Synthesis and Characterization of Mn Oxides

K-birnessite was synthesized by reducing 300 mL of 0.667 M $KMnO_4$ with 45 mL of 6 M HCl added at a rate of 0.7 mL/min under stirring at 110 °C, followed by aging at 60 °C for 16 h.[31] Vernadite was prepared by reducing a mixture of 750 mL of 0.1 M $KMnO_4$ and 0.2 M NaOH with 750 mL of 0.15 M $Mn(NO_3)_2$ added at 10 mL/min, followed by aging at 25 °C for 20 h under stirring.[32] Cryptomelane was synthesized by reducing 80 mL of 0.4375 M $KMnO_4$ with a mixture of 100 mL of 0.5 M $MnSO_4$ and 2 M acetic acid, followed by aging at 100 °C for 20 min and subsequently at 60 °C for 24 h.[31] For comparison with Mn(IV) oxides, Mn(III)-bearing manganite was synthesized by oxidizing a mixture of 200 mL of 0.7 M $MnSO_4$ and 0.2 M $NH_3{\cdot}H_2O$ with 90 mL of H_2O_2 at an addition rate of 3 mL/min at 95 °C, followed by aging under reflux at 105 °C for 24 h.[33] All synthesized Mn oxides were thoroughly washed with deionized water until the conductivity of the supernatant was below 20 μS/cm, and were then dried, ground, and passed through a 100-mesh sieve. Detailed synthesis procedures and physicochemical characterization methods, including X-ray diffraction (XRD), elemental composition, Mn oxidation state determined by XANES spectroscopy, N_2 adsorption−desorption isotherms, zeta potential measurements, and oxidation−reduction potential (ORP) analysis, are provided in the Supporting Information (Text S1).

2.2. Glyphosate Degradation Experiments

Glyphosate (CAS 1071-83-6, Aladdin, Shanghai) degradation kinetics by Mn oxides were conducted in duplicate at pH 3−7 and room temperature (22 ± 0.5 °C) over 2 h using 0.01 M NaCl as the background electrolyte to evaluate short-term degradation behavior. Reactions were initiated by rapidly mixing 100 mL of glyphosate stock solution (100 mg/L) with 100 mL of a pre-equilibrated Mn oxide suspension (0.4 g/L) in a 250 mL conical flask, resulting in final concentrations of 50 mg/L glyphosate and 0.2 g/L Mn oxide. This glyphosate/Mn ratio was selected based on both redox efficiency and environmentally relevant proportions.[34] Although the concentrations

https://doi.org/10.1021/acs.est.6c00923
Environ. Sci. Technol. 2026, 60, 25686−25700

Table 1. Specific Surface Areas and Pore Structure Parameters of Mn Oxides

	Micropore surface area (m^2/g)	External surface area (m^2/g)	Specific surface area (m^2/g)	Micropore volume (cm^3/g)	Total pore volume (cm^3/g)	Average pore size (nm)
Birnessite	6.6	19.5	26.1	0.002	0.193	11.4
Vernadite	32.3	299.6	331.8	0.016	0.619	4.5
Crytomelane	5.0	130.5	135.4	0.006	0.897	19.4

exceeded typical environmental levels, they are commonly employed in mechanistic studies to ensure measurable reaction kinetics and product formation.[4,21,35,36] The reactions were performed at pH 3, 5, and 7 under continuous magnetic stirring at 500 rpm, and the pH was maintained within ±0.1 units using 0.01 or 0.1 M HCl or NaOH. At predetermined time intervals, 5 mL aliquots were withdrawn and immediately filtered through 0.22 μm membrane filters. Glyphosate concentrations in the filtrate were quantified by sodium nitrite UV−vis spectrophotometry at 242 nm (Agilent Cary8454, USA),[37] and dissolved Mn concentrations were measured by atomic absorption spectroscopy (AAS; Agilent 204DUO).

To facilitate the identification of degradation intermediates and products, additional experiments were performed at elevated reactant concentrations (100 mg/L glyphosate and 0.5 g/L Mn oxides) with an extended reaction time of 24 h at pH values of 3, 5, and 7. The degradation kinetics of the primary metabolite AMPA (CAS 1066-51-9, Aladdin) were also evaluated under the same experimental conditions. Filtered samples were analyzed for AMPA and potential intermediates (e.g., sarcosine (CAS 107-97-1, Aladdin) and glycine (CAS 56-40-6, Aladdin)) using high-performance liquid chromatography (HPLC; Agilent 1260) with precolumn derivatization, following an established protocol.[38] Quantification was based on external calibration curves, and all measurements were conducted in duplicate with mean values reported. Detailed derivatization procedures and chromatographic conditions are described in Text S2. Glyphosate and phosphate concentrations were additionally determined by UV−vis spectrophotometry at 242 and 710 nm, respectively. After the reaction, solid residues were collected by filtration, freeze-dried, and finely ground for subsequent solid-phase characterization.

2.3. Identification of Reactive Species

2.3.1. Detection of Mn(III) Intermediates. The formation of soluble Mn(III) intermediates was examined using sodium pyrophosphate (PP) as a stabilizing chelating ligand.[39] Briefly, 5 mM PP was added to glyphosate degradation systems containing 0.2 g/L Mn oxide and 50 mg/L glyphosate, and to Mn oxide-only control suspensions, at pH 7.0. The mixtures were continuously stirred for up to 24 h. At predetermined time points, 2 mL aliquots were filtered through 0.22 μm membrane filters, and Mn(III)-PP complexes were quantified by UV−vis spectroscopy over a wavelength range of 200−600 nm, with the characteristic absorption peak monitored at approximately 258 nm.[39,40]

2.3.2. Identification of Reactive Oxygen Species (ROS). ROS generated by Mn oxides were examined using electron paramagnetic resonance (EPR) spectroscopy with 5,5-dimethyl-1-pyrroline N-oxide (DMPO) as a spin-trapping agent. Mn oxide suspensions (0.2 g/L) were prepared in 0.01 M NaCl at pH 3 and 7 and stirred for 2 h in the absence of glyphosate. Subsequently, 1 mL of the suspension was mixed with 10 μL of 25 mM DMPO for 2 min, filtered through a 0.22 μm membrane filter, and immediately analyzed by EPR spectroscopy (Bruker EMXnano) to identify DMPO-radical adducts.[41]

2.3.3. Quantification of Hydroxyl Radicals (•OH). The formation of •OH was quantified using terephthalic acid (TPA) as a fluorescent probe. Reaction mixtures containing 0.2 g/L Mn oxides and 0.2 mM TPA in 0.01 M NaCl were adjusted to pH 3, 5, and 7. TPA reacts selectively with •OH to form highly fluorescent 2-hydroxyterephthalic acid (hTPA).[42] At predetermined time intervals, 2 mL aliquots were filtered and analyzed by HPLC (Agilent 1260) equipped with a fluorescence detector and a Zorbax Eclipse SB-C18 column. The mobile phase consisted of 20% acetonitrile and 80% phosphoric acid solution (0.1 wt %) at a flow rate of 0.5 mL/min.

2.4. Characterization of Solid Products

Postreaction solids were characterized using multiple complementary analytical techniques. XRD patterns were collected to evaluate potential structural changes (see Text S1). For scanning electron microscopy (SEM; SU8010), freeze-dried samples were mounted on carbon tape, sputter-coated with gold, and imaged at 15 kV under a vacuum of 80 Pa.

XPS analyses were performed using a Thermo Fisher Scientific K-Alpha spectrometer equipped with a monochromatic Al Kα X-ray source (1486.6 eV). Survey spectra were collected at 100 eV pass energy (step size: 1.0 eV), and high-resolution scans (e.g., Mn 3s, Mn 2p, O 1s, and P 2p) were collected at 25 eV pass energy (step size: 0.1 eV). All spectra were charge-corrected using the adventitious carbon C 1s peak at 284.8 eV and processed using Avantage software. Detailed procedures for background subtraction, peak deconvolution, and Mn oxidation state determination are provided in the Supporting Information (Text S3 and Figure S1) following established methods.[43,44]

P K-edge XANES spectroscopy was conducted at beamline BL4B7A of the Beijing Synchrotron Radiation Facility (BSRF), enabling differentiation of organic and inorganic P species even at relatively low P loadings. Solid samples collected after glyphosate or AMPA degradation at pH 3 and 7, together with pure glyphosate and AMPA reference compounds, were analyzed. To minimize self-absorption effects, samples were diluted with boron nitride (BN) to achieve 15,000−20,000 mg P/kg. All samples were uniformly spread on P-free carbon tape, and spectra were collected in fluorescence mode using a Si(Li) detector. Each sample was scanned twice to improve the signal-to-noise ratio. Data processing, including background subtraction and normalization, was performed using the Athena software package.[45] Spectral analyses focused on the energy range of 2140−2180 eV.

In situ ATR-FTIR spectroscopy was employed to monitor glyphosate adsorption species on Mn oxides and the influence of Mn^{2+} at pH 5 and 7 using a Bruker Vertex 70 spectrometer. Briefly, 1 mL of 10 g/L mineral suspension was evenly deposited onto a ZnSe crystal and air-dried overnight. After establishing a stable baseline with 0.01 M NaCl at a flow rate of 1 mL/min, background spectra were collected. Subsequently, 1 mM glyphosate was introduced at the same flow rate for 60 min, followed by the addition of 10 mg/L (∼0.18 mM) $MnCl_2$ for an additional 60 min. The spectra at different time points were collected as averages of 256 scans at 4 cm^{-1} resolution over the spectral range of 800−1800 cm^{-1}.

3. RESULTS AND DISCUSSION

3.1. Structure-Dependent Physicochemical Properties of Synthesized Mn Oxides

XRD patterns confirmed the successful synthesis of the target Mn oxide phases, with crystallinity decreasing in the order K-birnessite (PDF#43-1456) > cryptomelane (PDF#42-1348) > vernadite (Figure S2a). Vernadite exhibited two broad and weak diffraction peaks characteristic of poorly crystalline δ-MnO_2.[32] The stoichiometries of the three Mn oxides were calculated based on elemental compositions and bulk Mn oxidation states determined by Mn K-edge XANES spectroscopy: $K_{0.10}Mn(IV)_{0.92}Mn(III)_{0.06}Mn(II)_{0.02}O_{2.04}\cdot 0.50H_2O$ for birnessite, $Na_{0.07}K_{0.06}Mn(IV)_{0.87}Mn(III)_{0.12}Mn(II)_{0.01}O_{2.00}\cdot 1.14H_2O$ for vernadite, and $K_{0.16}Mn(IV)_{0.84}Mn(III)_{0.14}Mn(II)_{0.02}O_{2.09}\cdot 0.61H_2O$ for cryptomelane. Pronounced differ-

https://doi.org/10.1021/acs.est.6c00923
Environ. Sci. Technol. 2026, 60, 25686−25700

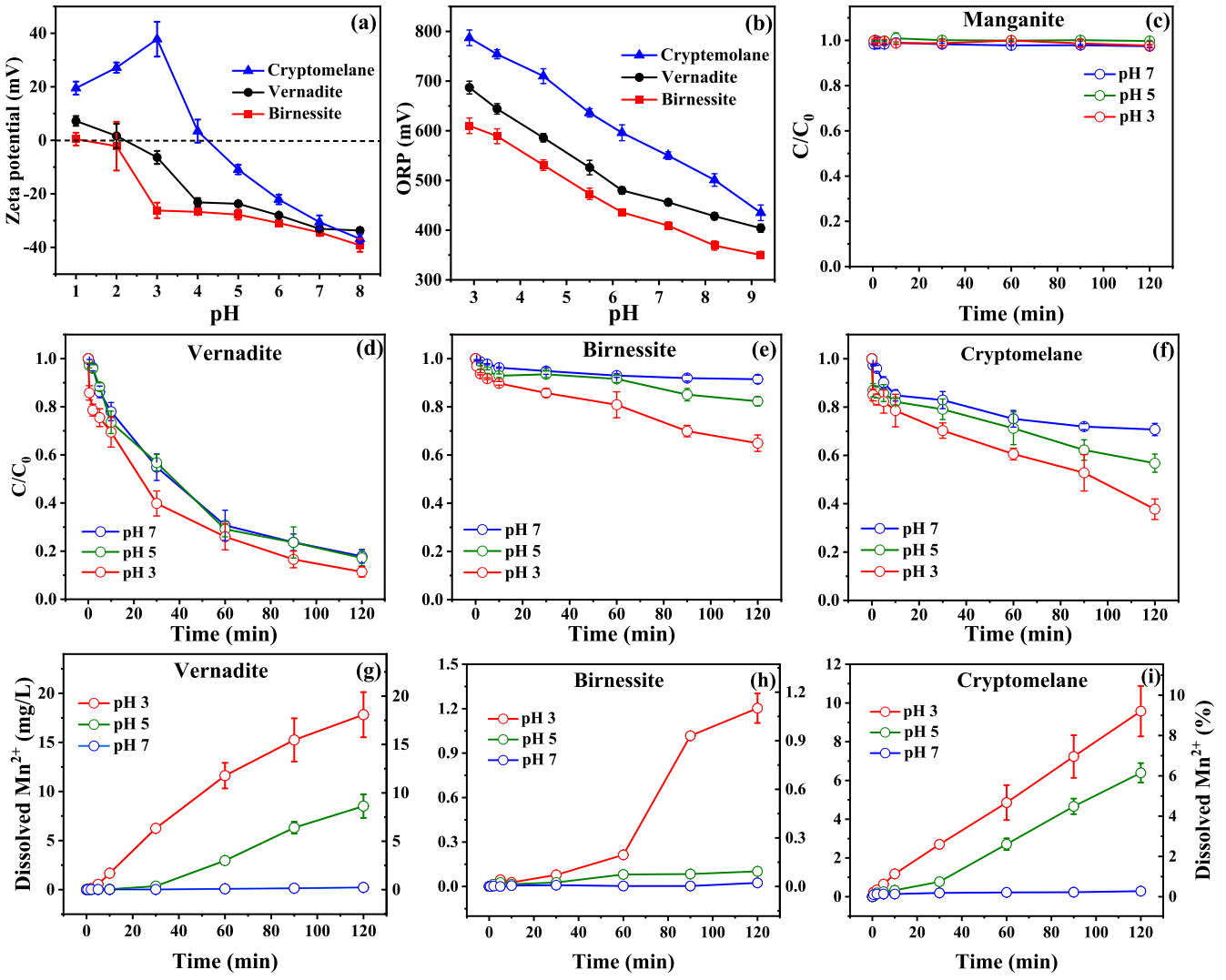

Figure 1. Zeta potential (a) and redox potential (b) of the synthesized Mn oxides. Glyphosate degradation kinetics by manganite (c), vernadite (d), birnessite (e), and cryptomelane (f), and the corresponding dissolved Mn release (including the percentage of the initial Mn; g–i) at pH 3, 5, and 7. The initial glyphosate concentration was 50 mg/L, the Mn oxide loading was 0.2 g/L, and the background electrolyte was 0.01 M NaCl.

Table 2. Surface Speciation of Mn and O, and Average Mn Oxidation States of Mn Oxides before and after Glyphosate Degradation, as Determined by XPS

Sample	Mn(II) (%)	Mn(III) (%)	Mn(IV) (%)	O_{ads} (%)	O_{latt} (%)	O_{ads}/O_{latt}	ΔE (eV)	AOS[a]
Birnessite	5.6	16.8	77.6	14.2	79.3	0.2	4.6	3.7
After reaction	5.8	33.3	60.9	16.0	66.0	0.2	4.9	3.4
Vernadite	6.9	32.5	60.6	19.0	67.5	0.3	4.9	3.4
After reaction	6.5	44.5	49.0	22.0	63.9	0.3	5.0	3.3
Cryptomelane	6.1	32.8	61.1	18.8	72.2	0.3	4.8	3.5
After reaction	6.4	47.5	46.1	22.9	60.4	0.4	4.9	3.4

[a]AOS: average oxidation state, AOS = 8.956 − 1.126 × ΔE, where ΔE represents the binding energy difference between the two peaks in the Mn 3s spectrum.[66]

ences in textural properties were observed among the three Mn oxides, as revealed by N_2 adsorption–desorption analyses and SEM observations (Figures S2b and S3; Table 1). Birnessite exhibited a predominantly mesoporous structure with pore diameters centered at 10–30 nm. In contrast, vernadite was predominantly microporous (<2 nm), with minor mesopores (2–3 nm), yielding the highest SSA (332 m^2/g). Cryptomelane displayed larger mesopores (20–45 nm) and an intermediate SSA (135 m^2/g), whereas birnessite possessed the lowest SSA (26 m^2/g). Morphologically, birnessite formed nanoflower-like aggregates, vernadite exhibited similar but 3–4-fold smaller spherical particles, and cryptomelane exhibited a needle-like morphology (Figure S3).

Surface charge measurements further highlighted pronounced structure-dependent differences among the Mn oxides. The PZC decreased in the order cryptomelane (pH 4.3) > vernadite (pH 2.2) > birnessite (pH 1.0) (Figure 1a), indicating progressively negative surface charge from crypto-

https://doi.org/10.1021/acs.est.6c00923
Environ. Sci. Technol. 2026, 60, 25686–25700

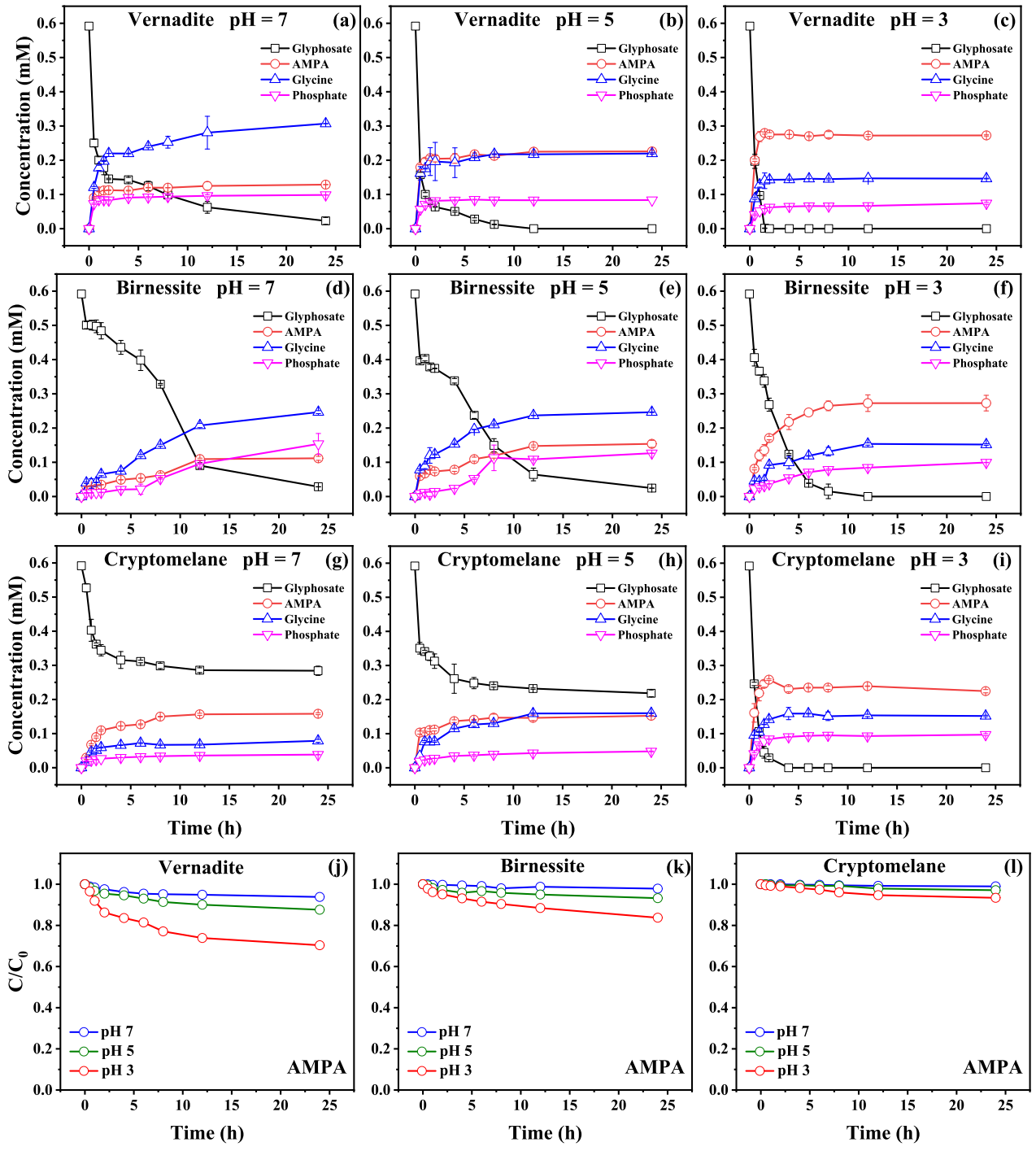

Figure 2. Time-dependent glyphosate degradation and the formation of primary transformation products during oxidation by vernadite (a−c), birnessite (d−f), and cryptomelane (g−i), and AMPA degradation kinetics by vernadite (j), birnessite (k), and cryptomelane (l) at pH 3, 5, and 7, as determined by HPLC. Initial glyphosate and AMPA concentrations were 100 mg/L, the Mn oxide loading was 0.5 g/L, and the background electrolyte was 0.01 M NaCl.

melane to birnessite over the environmentally relevant pH range (≤7). Redox potential measurements showed that all Mn oxides exhibited stronger oxidative potentials under acidic conditions, following the order cryptomelane > vernadite > birnessite (Figure 1b). This trend suggests that cryptomelane possessed the strongest intrinsic oxidative capacity among the investigated Mn oxides.

XPS analysis provided complementary information on the Mn oxidation states within the near-surface region (several nm depths; Table 2). The relative abundance of Mn(IV) followed the order birnessite > cryptomelane ≈ vernadite, whereas Mn(III) abundance showed an opposite trend. The Mn average oxidation state (AOS) calculated from XPS spectra aligned well with their respective Mn(IV) contents (Table 2). Mn K-edge XANES analyses showed a similar trend in Mn AOS to XPS among the three Mn oxides (Figure S4 and Table S1). However, XANES generally yielded slightly higher Mn(IV) fractions and AOS values, likely reflecting its greater

https://doi.org/10.1021/acs.est.6c00923
Environ. Sci. Technol. 2026, 60, 25686−25700

probing depth and bulk-sensitive nature. In addition, the proportion of adsorbed oxygen species (O_{ads}), including hydroxyl groups and molecularly adsorbed water, followed the order vernadite (19.0%) > cryptomelane (18.8%) > birnessite (14.2%), broadly reflecting differences in SSA (Table 1). Collectively, these distinct structural, surface, and redox characteristics provide a physicochemical basis for structure-dependent glyphosate adsorption, interfacial electron transfer, and subsequent oxidative transformation pathways.

3.2. Glyphosate Degradation Kinetics and pH Dependence

Batch experiments demonstrated that Mn(III)-bearing manganite exhibited negligible reactivity toward glyphosate (Figure 1c), whereas all three Mn(IV) oxides effectively oxidized glyphosate (Figure 1d–f). This contrast indicates that the mere presence of structural Mn(III) is insufficient to drive glyphosate oxidation under the tested conditions, highlighting Mn(IV) as the primary oxidizing species. Among the Mn(IV) oxides, glyphosate degradation efficiency consistently followed the order vernadite > cryptomelane > birnessite across all pH conditions (Figure 1d–f). Kinetic data were well fitted by a pseudo-first-order model (R_2 = 0.86–0.98), yielding apparent rate constants (k) of 0.0150–0.0176 min^{-1} for vernadite, 0.0028–0.0065 min^{-1} for cryptomelane, and 0.0007–0.0033 min^{-1} for birnessite over pH 3–7 (Table S2).

Solution pH exerted a pronounced control over glyphosate degradation kinetics. Under acidic conditions (pH 3), both cryptomelane and vernadite exhibited rapid initial degradation, achieving approximately 15.0% glyphosate removal within the first 0.5 min (Figure 1d and f). After 120 min, vernadite achieved the highest glyphosate removal efficiency (88.6%), followed by cryptomelane (62.3%) and birnessite (35.1%). Increasing pH systematically suppressed glyphosate degradation for all Mn oxides (Figure 1d–f). Cryptomelane displayed the strongest pH sensitivity, with removal efficiency decreasing from 62.3% at pH 3 to 30.2% at pH 7. In contrast, vernadite maintained high reactivity even at neutral pH (82.1% removal), whereas birnessite showed limited reactivity at a pH of 7 (8.6% removal).

Glyphosate oxidation was accompanied by the reductive dissolution of Mn oxides, resulting in the release of dissolved Mn (Figure 1g–i), predominantly as Mn(II) with minor contributions from Mn(III).[22] The accumulation of dissolved Mn closely paralleled glyphosate degradation efficiency, following the order vernadite > cryptomelane > birnessite under each pH condition. As pH decreased to 3, the dissolved Mn concentration increased to 17.82 mg/L (0.32 mM, 18%), 9.58 mg/L (0.17 mM, 9%), and 1.20 mg/L (0.02 mM, 1%) for vernadite, cryptomelane, and birnessite, respectively. The pH dependence likely reflects both enhanced interfacial redox kinetics under acidic conditions and reduced adsorption of dissolved Mn on increasingly protonated Mn-oxide surfaces.[46]

Overall, the kinetic trends indicate that glyphosate degradation is strongly favored under acidic conditions and is governed by the coupled effects of Mn oxide surface charge, oxidative potential, and glyphosate speciation. As the pH increases from 3 to 7, Mn oxide surfaces become increasingly negatively charged (Figure 1a), their redox potentials decrease (Figure 1b) and glyphosate predominantly exists as multivalent anionic species due to deprotonation of its phosphonate group (pK_{a1} = 2.2, pK_{a2} = 5.4, pK_{a3} = 10.1),[47] collectively enhancing electrostatic repulsion and inhibiting surface complexation and interfacial electron transfer. In contrast, lower pH facilitates glyphosate adsorption, proton-assisted electron transfer, and Mn(IV) reduction at Mn oxide surfaces, as represented by the following reactions (eqs 13):

$$MnO_2 + e^- + H^+ \rightarrow Mn(III)OOH \quad (1)$$

$$MnO_2 + 2e^- + 4H^+ \rightarrow Mn(II) + 2H_2O \quad (2)$$

$$MnO_2 + Mn(II) + 2H^+ \rightarrow 2Mn(III) + 2H_2O \quad (3)$$

Notably, at pH 3, cryptomelane possessed a net positive surface charge (pH < PZC), whereas vernadite and birnessite remained negatively charged (Figure 1a). Despite its lower SSA, cryptomelane exhibited an initial degradation rate comparable to that of vernadite (Figure 1f), likely attributable to its higher intrinsic redox potential combined with favorable electrostatic attraction toward glyphosate (Figure 1a–b). Compared with birnessite and cryptomelane, the degradation rate of glyphosate on vernadite was less sensitive to pH, likely because its exceptionally high SSA (Table 1) enabled sustained glyphosate adsorption and oxidation even under near-neutral conditions.

3.3. Degradation Products and Pathways of Glyphosate

3.3.1. Evolution of Intermediates and Final Products.

To elucidate complete degradation pathways and resolve transient intermediates, long-term experiments were conducted using elevated reactant concentrations (100 mg/L glyphosate, 0.5 g/L Mn oxide) over 24 h. The overall removal trends (Figure 2a–i) were broadly consistent with the kinetic behaviors observed at lower reactant concentrations (Figure 1d–f), while more clearly revealing structure-dependent controls on glyphosate persistence and product evolution. Vernadite displayed the fastest and most sustained reactivity, whereas birnessite exhibited slower initial kinetics; nevertheless, both achieved nearly complete glyphosate removal after 24 h across the whole pH 3–7 range (Figure 2a–f). In contrast, cryptomelane exhibited pronounced pH dependence, achieving complete glyphosate removal within 4 h at pH 3 but only ~52% after 24 h at pH 7 (Figure 2g and i). Notably, birnessite outperformed cryptomelane at higher pH (5–7), indicating that initial degradation rates do not necessarily correspond to greater long-term oxidative capacity.

The primary metabolite AMPA exhibited substantially greater persistence than glyphosate (Figure 2j–l), consistent with its higher intrinsic chemical stability.[20] AMPA oxidation was most efficient under acidic conditions, where Mn oxides exhibited stronger oxidative capacity and higher adsorption affinity for AMPA with less negative charge (pK_{a1} = 1.8, pK_{a2} = 5.4, pK_{a3} = 10.0),[48] with vernadite consistently showing the highest reactivity. Cryptomelane was the least effective oxide for AMPA oxidation, confirming that the Mn oxide structure exerts sustained control on both primary glyphosate degradation and secondary AMPA transformation.

Distinct degradation pathways were evident from the temporal evolution of reaction intermediates. In the vernadite system at pH 7, both AMPA and glycine accumulated over time, with glycine remaining the dominant product throughout the reaction (Figure 2a). As the pH decreased, AMPA formation became progressively favored and persisted throughout the reaction. At pH 5, AMPA and glycine were produced in comparable amounts, whereas glycine formation was markedly suppressed at pH 3 (Figure 2b–c). Birnessite exhibited similar pathway preferences but with substantially

https://doi.org/10.1021/acs.est.6c00923
Environ. Sci. Technol. 2026, 60, 25686–25700

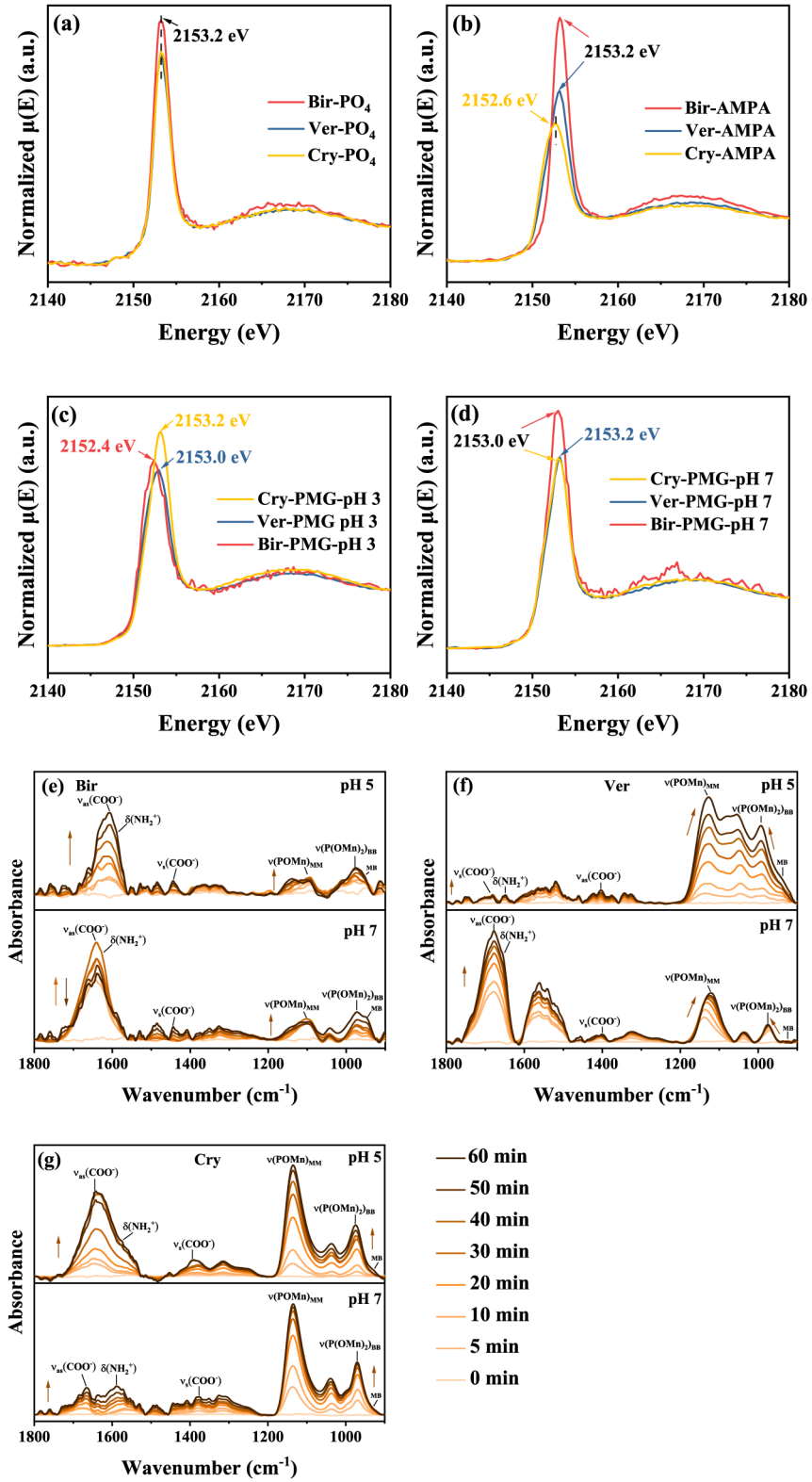

Figure 3. P K-edge XANES spectra of Mn oxides preloaded with phosphate (a) and AMPA (b), and of solid residues collected after glyphosate degradation by cryptomelane (Cry), vernadite (Ver), and birnessite (Bir) at pH 3 (c) and pH 7 (d). Experiments were conducted with an Mn oxide loading of 0.5 g/L, and initial concentrations of phosphate, AMPA, and glyphosate of 100 mg/L. In situ ATR-FTIR spectra of glyphosate adsorption on birnessite (e), vernadite (f), and cryptomelane (g) within 60 min at pH 5 and 7. MM, BB, and MB denote monodentate mononuclear, bidentate binuclear, and mononuclear bidentate surface complexes, respectively.

slower reaction kinetics (Figure 2d–f). At pH 7 and 5, both glycine and AMPA gradually accumulated, although glycine remained the dominant product, reaching 0.25 mM after 24 h at both pH values, whereas AMPA concentrations reached only 0.11 and 0.15 mM, respectively (Figure 2d–e). At lower pH, AMPA accumulation was again enhanced, whereas glycine

https://doi.org/10.1021/acs.est.6c00923
Environ. Sci. Technol. 2026, 60, 25686−25700

yields were reduced (Figure 2f). These results are consistent with previous studies showing glycine as the dominant degradation product on birnessite at pH 4.6−7.2, with the contribution of the AMPA pathway increasing as pH decreases.[21,22,35] In contrast to layered Mn oxides, cryptomelane predominantly favored the AMPA pathway across all pH conditions, producing comparatively smaller amounts of glycine (Figure 2g−i). At pH 3, AMPA concentrations rapidly peaked (0.26 mM at 2 h) and subsequently declined to 0.22 mM after 24 h (Figure 2i), providing direct evidence for secondary AMPA adsorption and oxidation under strongly acidic conditions.

Phosphate release patterns further highlighted the coupled effects of the Mn oxide structure and pH on degradation pathways. For layered Mn oxides, phosphate concentrations increased with pH, reaching 0.15 mM (25% of the initial total P) for birnessite and 0.10 mM (17% of the initial P) for vernadite at pH 7 after 24 h, while remaining relatively lower at pH 3 (Figure 2a and d). At a lower pH, the layered Mn oxide surface and phosphate species (pK_1 = 2.2 and pK_2 = 7.2) carried less negative charge (Figures 1a and S5),[49] thereby favoring phosphate adsorption onto mineral surfaces. In contrast, cryptomelane released up to 0.10 mM (17% of the initial P) phosphate at pH 3, coinciding with complete glyphosate oxidation (Figure 2i). At pH 7, limited glyphosate degradation by cryptomelane was accompanied by minimal phosphate release (Figure 2g). The total quantified P-bearing products (AMPA, glycine-equivalent methylphosphonic acid, and phosphate) were slightly lower than the amount of glyphosate degraded, particularly at pH 3, likely because a fraction of the products remained adsorbed on mineral surfaces (Figure S6).

3.3.2. Molecular-Scale Speciation of Surface-Bound Phosphorus. P K-edge XANES spectroscopy was employed to elucidate P speciation on Mn oxide surfaces following glyphosate degradation. Spectra of postreaction solids (Figure 3c−d) were compared with those of phosphate- or AMPA-sorbed Mn oxide (Figure 3a−b) and pure glyphosate and AMPA standards (Figure S7). The white-line peaks of pure glyphosate and AMPA both occurred at 2151.2 eV (Figure S7), whereas those of Mn oxide-associated samples shifted to higher energies (Figure 3a−d), indicating the formation of P−O−Mn inner-sphere surface complexes.[50]

For phosphate-sorbed samples, all Mn oxides exhibited a characteristic white-line peak at 2153.2 eV (Figure 3a). Birnessite showed the highest peak intensity, which, given the inverse relationship between peak intensity and adsorbed P loading,[51] indicates the lowest phosphate adsorption, consistent with its low SSA (Table 1). In AMPA-sorbed samples, vernadite and birnessite exhibited identical white-line energies (2153.2 eV), suggesting extensive oxidation of AMPA to phosphate on these oxide surfaces. In contrast, cryptomelane exhibited a slightly lower white-line energy (2152.6 eV) accompanied by broader peak features (Figure 3b), implying a greater fraction of unoxidized AMPA and a more heterogeneous mixture of organic and inorganic P species.[52] These spectroscopic features are consistent with macroscopic degradation results (Figure 2j−l), confirming that the Mn oxide structure governs both AMPA persistence and transformation efficiency.

At pH 3, where glyphosate was almost completely degraded within 24 h for all Mn oxides (Figure 2c, f, and i), the white-line peak energies of the postreaction solids followed the order cryptomelane > vernadite > birnessite (Figure 3c). This trend closely paralleled the extent of phosphate release into the solution. Cryptomelane, which released the largest amount of phosphate, exhibited the highest white-line energy (2153.2 eV), reflecting the predominance of surface-bound phosphate species. In contrast, birnessite displayed the lowest white-line peak energy (2152.4 eV), likely due to competitive adsorption among phosphate, AMPA, and residual glyphosate on its limited reactive surface sites associated with its low SSA (Table 1). At pH 7, the white-line peak energies converged across all Mn oxides (2153.0−2153.2 eV, Figure 3d), despite pronounced differences in degradation efficiency and product distributions (Figure 2a, d, g). This convergence indicates that surface P speciation approached a similar adsorption equilibrium dominated by mixed phosphate and organic P complexes under near-neutral conditions.

In situ ATR-FTIR spectroscopy was further employed to investigate glyphosate adsorption configurations on Mn oxides at pH 5 and 7. The spectra showed prominent characteristic bands of carboxyl and amino groups at 1679−1573 cm^{-1}, as well as phosphonate groups at 920−1190 cm^{-1} (Figure 3e−g, Table S3), which intensified over time. Comparison of relative band intensities among the Mn oxides showed that birnessite and vernadite exhibited stronger carboxylate and amino bands than phosphonate bands at pH 7, whereas cryptomelane displayed more pronounced phosphonate bands. At pH 5, the phosphonate band intensity in vernadite exceeded that of carboxylate and amino groups, while only minor changes were observed for birnessite and cryptomelane (Figure 3e−g).

The phosphonate group of glyphosate formed monodentate mononuclear (1136−1093 cm^{-1}), mononuclear bidentate (954−923 cm^{-1}), and bidentate binuclear (979−970 cm^{-1}) surface complexes on the three Mn oxides.[22] On birnessite surfaces, glyphosate phosphonate primarily formed bidentate binuclear complexes (Figure 3e), consistent with previous studies.[22] On cryptomelane surfaces, glyphosate predominantly formed monodentate mononuclear complexes (Figure 3g). On vernadite surfaces, the monodentate mononuclear and bidentate binuclear bands gradually shifted over time from 1139 to 1120 cm^{-1} and from 970 to 974 cm^{-1} (Figure 3f), respectively, likely reflecting Mn(II) adsorption and progressive bond cleavage associated with the high reactivity of vernadite (Figure S8). Overall, these observations demonstrate that glyphosate adopts distinct adsorption configurations on layered and tunnel-structured Mn oxides, which in turn regulate interfacial electron transfer, degradation pathways, and product distributions.

3.3.3. Structure- and pH-Dependent Degradation Pathways. Glyphosate oxidation by Mn oxides can theoretically proceed via three primary pathways: (1) C(3)−P bond cleavage, yielding phosphate and sarcosine; (2) C(2)−N bond cleavage adjacent to the carboxyl group, generating AMPA and glyoxylic acid; and (3) C(3)−N bond cleavage adjacent to the phosphonate group, producing glycine and methylphosphonic acid.[10,20,35] In this study, glycine and AMPA were consistently identified as the dominant transformation intermediates. Additional degradation experiments at pH 5 showed that sarcosine (1.1 mM) was completely degraded by Mn oxides (0.5 g/L) within 0.5 h without detectable glycine formation. These observations indicate that glyphosate may partially degrade through the sarcosine pathway (Pathway 1); however, glycine formation primarily originated from direct C(3)−N

https://doi.org/10.1021/acs.est.6c00923
Environ. Sci. Technol. 2026, 60, 25686−25700

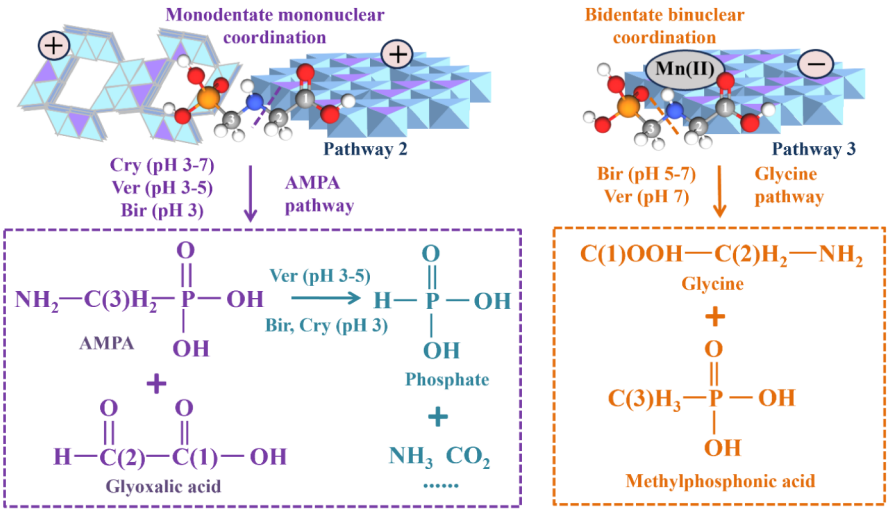

Figure 4. Conceptual schematic illustrating the predominant degradation pathways of glyphosate mediated by Mn oxides as a function of mineral structure and solution pH. Cry: cryptomelane; Ver: vernadite; Bir: birnessite.

bond cleavage (Pathway 3), rather than from secondary oxidation of sarcosine generated via C(3)−P bond cleavage.

The dominant degradation pathway was jointly governed by Mn oxide structure and solution pH. At near-neutral pH, layered Mn oxides (birnessite and vernadite) primarily facilitated the cleavage of the C−N bond adjacent to the phosphonate group, producing glycine as the dominant product (Pathway 3). In contrast, tunnel-structured cryptomelane favored the cleavage of the C−N bond near the carboxyl group, generating AMPA as the main product (Pathway 2) (Figures 2 and 4). This clear pathway divergence highlights a structure-dependent control over bond-selective oxidation of glyphosate.

This pathway selectivity can be explained by differences in surface complexation geometry and surface charge among the Mn oxides. On cryptomelane surfaces, glyphosate phosphonate predominantly forms monodentate mononuclear complexes (Figure 3g), favoring C(2)−N cleavage and subsequent AMPA formation (Pathway 2).[22] On vernadite surfaces, the relative abundance of bidentate binuclear complexes increased, resulting in lower AMPA yields. On birnessite surfaces, glyphosate phosphonate groups mainly formed bidentate binuclear complexes (Figure 3e), facilitating C(3)−N cleavage and glycine formation (Pathway 3) (Figure 4). The amino and carboxyl groups of glyphosate primarily adsorbed on negatively charged vacancy sites on layered Mn oxides due to their lower PZC and abundant basal Mn vacancies (Figures 1a and 3e−f).[53] This adsorption configuration likely stabilized the C(2)−N bond adjacent to the carboxyl group, thereby suppressing AMPA formation while favoring glycine production.[54] In contrast, cryptomelane lacks strongly negatively charged vacancy sites, and glyphosate predominantly binds through the phosphonate group to surface hydroxyl sites (Figure 3g), leading to preferential AMPA accumulation.

The observed pH dependence further supports this adsorption-controlled mechanistic interpretation. For layered Mn oxides, product selectivity shifted from AMPA dominance at pH 3 to glycine dominance at pH 7 (Figure 2a−f), coinciding with increasingly negative surface charge (Figure 1a) and stronger interactions between the carboxyl/amino groups and negatively charged vacancy sites at higher pH (Figure 3e−f). Conversely, in tunnel-structured cryptomelane, the absence of negatively charged sites maintained AMPA as the dominant product across all pH conditions (Figure 2g−i). Collectively, these results demonstrate that Mn oxide surface charge and glyphosate adsorption configurations are primary factors governing competition between the two C−N bond cleavage pathways.

The formation of phosphate despite the predominance of C−N bond cleavage pathways warrants further consideration. We propose that phosphate originated from two concurrent processes: (1) minor direct C−P bond cleavage during primary glyphosate oxidation and (2) subsequent oxidation of accumulated AMPA, which also contains a C−P bond. In contrast, methylphosphonic acid produced via pathway 3 appeared relatively resistant to Mn oxide-mediated oxidation and therefore contributed negligibly to phosphate formation.[35] The decline in AMPA concentrations at later reaction stages, particularly under acidic conditions (Figure 2c, f, i), together with its measurable degradation in independent AMPA oxidation experiments (Figure 2j−l), supports secondary AMPA oxidation as a major contributor to phosphate release, especially at low pH. Other potential degradation products of glyphosate generated by Mn oxides are summarized in Table S4.

3.4. Oxidation Mechanisms of Glyphosate by Mn Oxides

3.4.1. Direct Electron Transfer Dominated by Mn(III) Intermediates. Reductive dissolution of Mn(IV) oxides by organic compounds is commonly accompanied by the formation of soluble or labile Mn(III) species, which can function as highly reactive transient oxidants.[55,56] To evaluate the role of Mn(III) intermediates in glyphosate oxidation, PP was employed to stabilize labile Mn(III) species and enable their quantification via the characteristic UV−Vis absorption of Mn(III)−PP complexes.

The formation kinetics and accumulation of Mn(III) at pH 7 were strongly dependent on Mn oxide structure (Figure 5a−f). In the vernadite system, glyphosate addition induced the rapid appearance of a pronounced Mn(III)-PP absorbance peak within 0.5 h, followed by a sharp increase in intensity, indicating rapid and substantial Mn(III) production (Figure 5a). In the absence of glyphosate, Mn(III)-PP formation was still evident but with markedly lower intensity (Figure 5b),

https://doi.org/10.1021/acs.est.6c00923
Environ. Sci. Technol. 2026, 60, 25686−25700

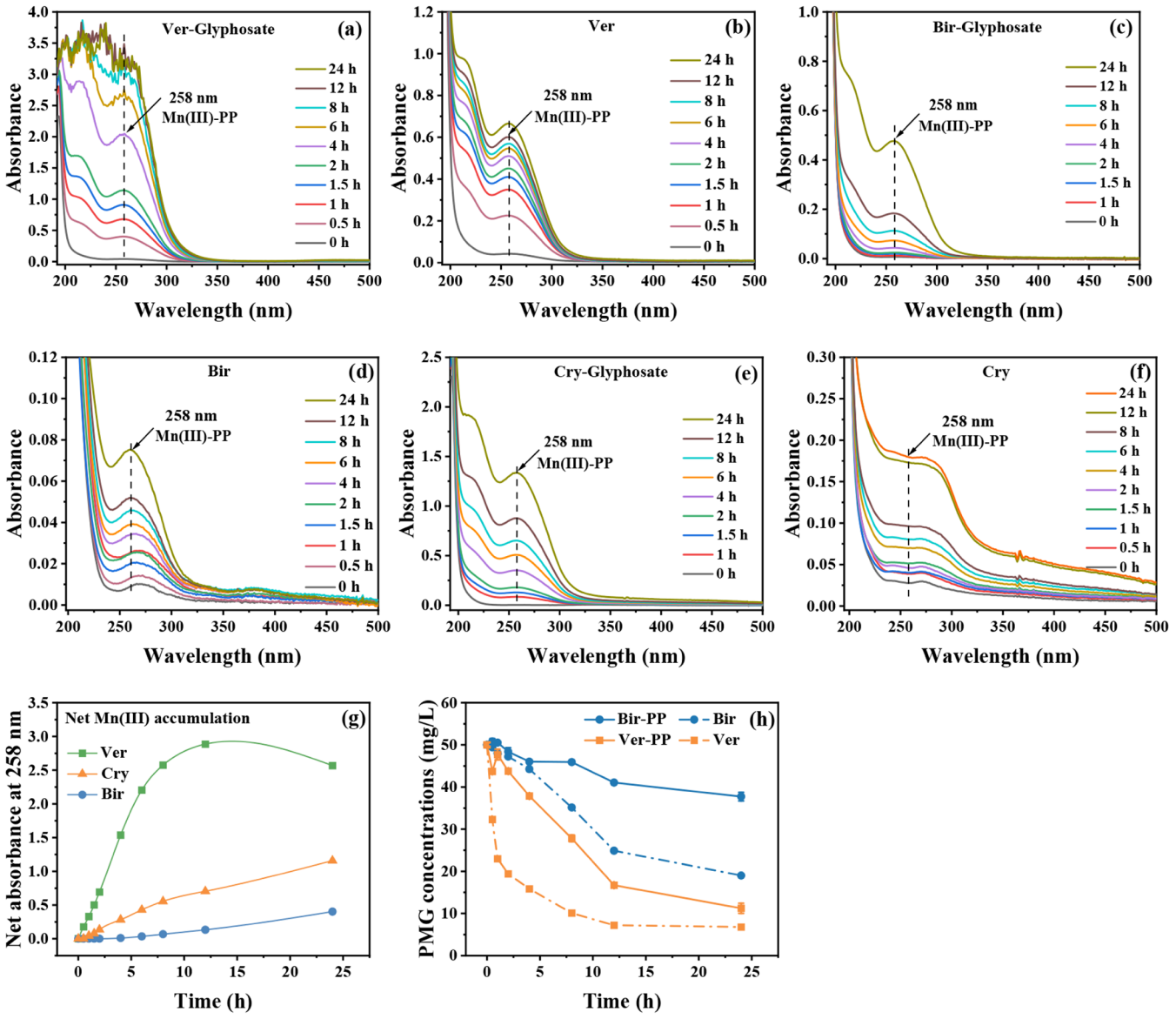

Figure 5. UV−vis absorption spectra of Mn(III)-PP complexes formed in Mn oxide systems in the presence (a, c, e) and absence (b, d, f) of glyphosate, and net Mn(III)-PP accumulation after subtraction of the glyphosate-free controls (g). Reaction conditions for panels (a−g): 0.2 g/L Mn oxides, 50 mg/L glyphosate, 5 mM PP, and pH 7 ± 0.1. Glyphosate degradation kinetics by Mn oxides in the presence and absence of 5 mM PP are shown in panel (h). Reaction conditions for panel (h): 0.2 g/L vernadite or 0.5 g/L birnessite with 50 mg/L glyphosate. Cry: cryptomelane; Ver: vernadite; Bir: birnessite.

indicating that organic oxidation strongly promotes Mn(III) generation. In contrast, birnessite displayed a delayed response, with detectable Mn(III) appearing only after 2 h in the presence of glyphosate and gradually increasing to a maximum at 24 h comparable to the early-stage (0.5 h) Mn(III) signal observed for vernadite (Figure 5c). Only trace Mn(III) formation was detected in the glyphosate-free birnessite system (Figure 5d). Cryptomelane showed intermediate behavior, with Mn(III) first detected at ∼1 h and reaching intensities between those of vernadite and birnessite, regardless of glyphosate presence (Figure 5e−f). Quantification of Mn(III) accumulation revealed a clear hierarchy of vernadite ≫ cryptomelane > birnessite (Figure 5g), consistent with their respective glyphosate degradation efficiencies (Figure 2). Importantly, the accumulated Mn(III) species primarily originated from redox reactions between Mn oxides and glyphosate rather than from preexisting structural Mn(III).

XPS analyses of post-reaction solids further corroborated these redox transformations (Figures 6 and S1 and Table 2). All Mn oxides exhibited a decrease in Mn(IV) content accompanied by an increase in Mn(III), while Mn(II) fractions remained relatively minor. The resulting decrease in Mn AOS was most pronounced for vernadite, consistent with its highest reactivity (Figure 6). Importantly, no phase transformations were observed, with only slight decreases in crystallinity occurring during the reaction (Figure S9).

Importantly, the addition of PP markedly suppressed glyphosate degradation by both vernadite and birnessite (Figure 5h). In the vernadite system, glyphosate degradation was consistently inhibited throughout the entire reaction in the presence of PP, reflecting the sustained sequestration of reactive Mn(III) intermediates. In contrast, PP exerted little influence on glyphosate degradation by birnessite during the initial reaction stage, consistent with the limited formation of

https://doi.org/10.1021/acs.est.6c00923
Environ. Sci. Technol. 2026, 60, 25686−25700

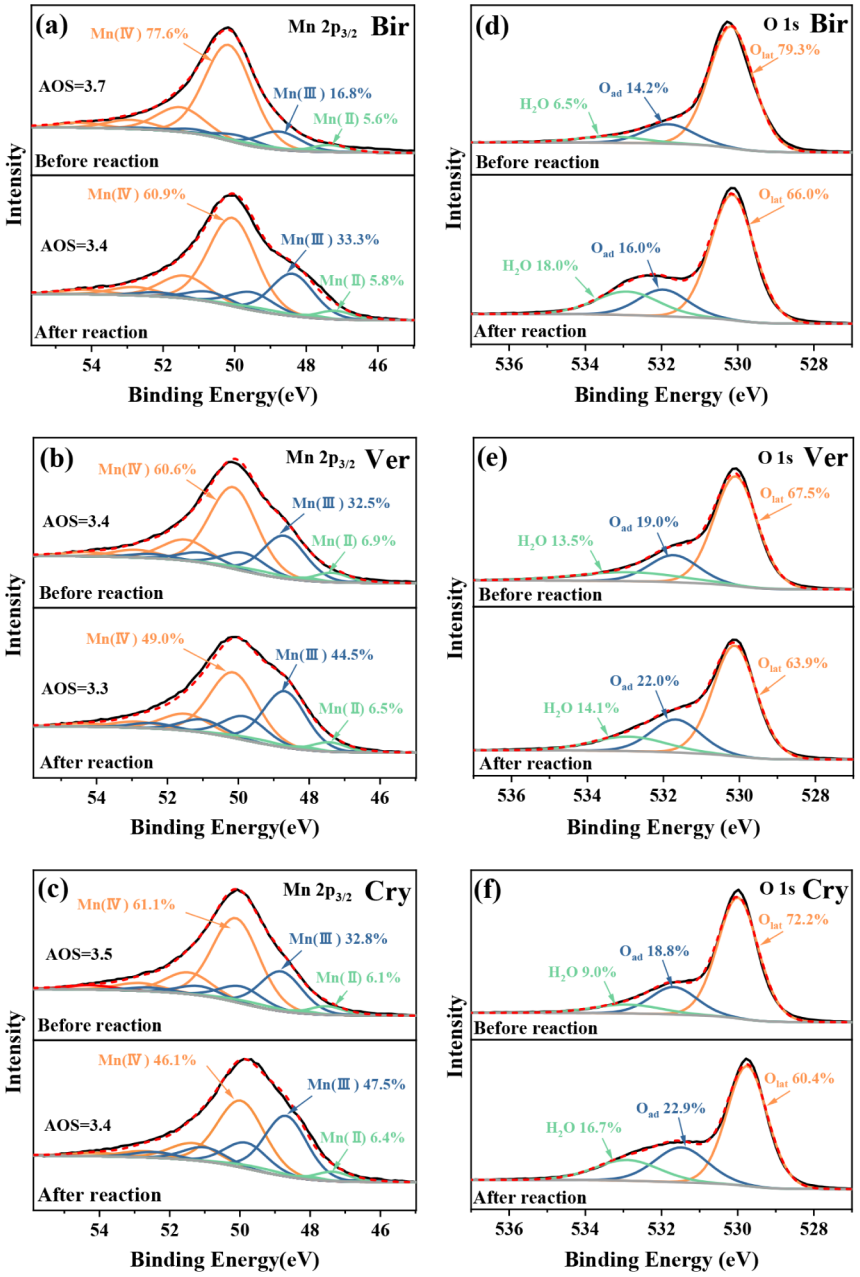

Figure 6. XPS spectra of Mn $2p_{3/2}$ (a: birnessite; b: vernadite; c: cryptomelane) and O 1s (d: birnessite; e: vernadite; f: cryptomelane) of Mn oxides before and after glyphosate degradation. Reaction conditions: 0.5 g/L Mn oxides, 100 mg/L glyphosate, 0.01 M NaCl, and pH 7 ± 0.1.

Mn(III) during this period (Figure 5c). As the reaction progressed, Mn(III) accumulation increased substantially, accompanied by a progressively stronger inhibitory effect of PP on the glyphosate degradation. Given the high SSA of vernadite, competitive adsorption between PP and glyphosate was unlikely to dominate the observed inhibition, indicating that inhibition primarily resulted from the chelation and stabilization of reactive Mn(III) species rather than surface site blocking. These observations provide direct evidence that soluble or labile Mn(III) intermediates play a central role in controlling glyphosate oxidation kinetics.[57]

Collectively, these results support a direct electron transfer mechanism governed by coupled Mn(IV)/Mn(III)/Mn(II) redox cycling (eqs 1−3). The process is initiated by surface complexation of glyphosate with Mn(IV) sites, followed by coupled one- and two-electron transfer processes that reduce structural Mn(IV) to Mn(III) and Mn(II). Adsorbed Mn(II) can subsequently undergo comproportionation with neighboring Mn(IV) to generate transient Mn(III) species.[57] These labile Mn(III) intermediates function as potent one-electron oxidants capable of diffusing over short distances, readsorbing onto mineral surfaces, or becoming incorporated into lattice vacancies, particularly abundant in layered Mn oxides, thereby sustaining continued glyphosate oxidation.[58,59] Morphological evidence of mineral restructuring, including edge dissolution and the formation of amorphous secondary phases (Figure S3), further supports dynamic redox cycling and mineral transformation during reaction.[60]

Because Mn(III) species have been implicated in ROS generation in related Mn oxide systems,[56] their potential contribution to glyphosate degradation was explicitly evaluated. EPR spectroscopy using DMPO spin trapping detected

https://doi.org/10.1021/acs.est.6c00923
Environ. Sci. Technol. 2026, 60, 25686−25700

only a DMPO−X signal, which was attributed to direct oxidation of DMPO by Mn oxides rather than to free radical generation (Figure S10). No DMPO−OH or DMPO−OOH signals indicative of •OH or O_2•$^-$ radicals were observed. This conclusion was further supported by terephthalic acid (TPA) fluorescence assays for •OH detection,[42] which showed no detectable formation of •OH over 24 h (Figure S11). Although minor radical contributions cannot be entirely excluded,[61] the consistent absence of ROS signatures across two complementary probes indicates that glyphosate degradation under the investigated conditions was dominated by direct electron transfer mediated by Mn oxides and Mn(III) intermediates rather than by radical-driven pathways. This interpretation is consistent with previous studies showing that Mn oxides mediate organic contaminant transformation predominantly through nonradical pathways under dark conditions.[62]

3.4.2. Structural Determinants of Degradation Reactivity. Oxidative degradation of organic pollutants by Mn oxides generally proceeds through two sequential steps: (1) adsorption and precursor complex formation at surface Mn(IV) sites, followed by (2) interfacial electron transfer.[63] Our results demonstrate that the Mn oxide mineral structure critically regulates both steps through a suite of interrelated physicochemical properties, including crystallinity, SSA, oxidative potential, and the capacity to generate labile Mn(III) intermediates.

Cryptomelane, characterized by a tunnel structure, exhibited rapid initial glyphosate degradation, particularly under acidic conditions (Figure 1f and Figure 2i). This behavior likely arises from its relatively high SSA and large mesopore size (20−45 nm), which facilitate diffusion of glyphosate molecules (~0.9 nm),[64] together with the highest intrinsic redox potential among the investigated Mn oxides (Table 1 and Figure 1b). These features collectively promote efficient surface complexation and rapid initial interfacial electron transfer. However, the high crystallinity of cryptomelane likely imparts structural rigidity that increases the energetic barrier for sustained redox turnover (Figure S2a).[65] As a result, its oxidative efficiency declined markedly under circumneutral conditions (pH 5−7), where long-term redox sustainability rather than initial reactivity becomes rate-limiting (Figure 2g and h).

In contrast, vernadite, a disordered layered Mn oxide, exhibited the highest overall degradation capacity across the investigated pH range (Figures 1a,d and 2a−c). Its exceptional performance arises from a synergistic combination of low crystallinity, exceptionally high SSA, and abundant reactive surface oxygen species (Figure S2a and Table 1). Although its redox potential is lower than that of cryptomelane, vernadite generated the largest amount of labile Mn(III) intermediates (Figure 5a and g). These Mn(III) species function as mobile one-electron oxidants that continuously propagate oxidation reactions beyond the initial Mn(IV) surface sites. The coupling of high adsorption capacity with prolific Mn(III) generation renders vernadite to be the most effective and sustainable oxidant among the examined Mn oxides.

Birnessite, another layered Mn oxide, displayed the slowest initial degradation kinetics, primarily due to its low SSA, limited porosity, and comparatively low oxidative potential (Table 1, Figure 1a−b, S2c). Nevertheless, birnessite possesses the highest Mn AOS (Table 2), reflecting a substantial reservoir of structural Mn(IV). This intrinsic oxidative capacity enables birnessite to sustain oxidation over extended reaction periods, ultimately achieving complete glyphosate degradation and surpassing cryptomelane under circumneutral conditions (Figures 2d and g). These observations suggest that birnessite reactivity is initially constrained by surface complexation kinetics but is increasingly governed by persistent Mn(IV)-driven oxidation as the reaction progresses.

Collectively, the observed structure-dependent reactivity reflects a dynamic interplay between the surface accessibility and long-term redox sustainability. Cryptomelane excels in rapid initial oxidation due to its high oxidative potential and accessible tunnel framework; vernadite combines an extensive reactive surface area with prolific Mn(III) generation to sustain rapid and efficient oxidation; and birnessite relies on its large Mn(IV) reservoir to maintain long-term oxidative capacity. This mechanistic framework provides a predictive basis for linking Mn oxide mineralogy to oxidation kinetics, pathway selectivity, and contaminant transformation outcomes in both natural and engineered environments.

4. ENVIRONMENTAL IMPLICATIONS

This study establishes a comprehensive mechanistic framework for glyphosate degradation by Mn oxides, explicitly linking Mn oxide mineralogy and solution pH to reaction kinetics, transformation pathways, and interfacial redox mechanisms. Within the investigated pH range (3−7), glyphosate degradation efficiency followed the order vernadite > cryptomelane > birnessite and was markedly enhanced under acidic conditions. Under near-neutral conditions, layered Mn oxides (birnessite and vernadite) preferentially cleaved the C−N bond adjacent to the phosphonate group, forming glycine as the dominant product, whereas tunnel-structured cryptomelane favored cleavage near the carboxyl group, leading to AMPA accumulation. Under acidic conditions, AMPA formation was consistently enhanced across all Mn oxides, indicating an elevated risk of AMPA persistence in acidic soils and sediments.

Mechanistically, glyphosate oxidation was dominated by direct electron transfer mediated by structural Mn(IV) and transient, labile Mn(III) intermediates rather than by radical-driven pathways. The formation and persistence of Mn(III) emerged as critical controls on sustained oxidative reactivity, with vernadite generating the highest abundance of reactive Mn(III) intermediates and exhibiting the greatest overall oxidative reactivity. The contrasting behaviors of individual Mn oxides reflect distinct structure−reactivity relationships: vernadite combines exceptionally high SSA with prolific Mn(III) generation to sustain rapid and efficient oxidation; cryptomelane couples high intrinsic oxidative potential with accessible tunnel porosity to drive rapid initial degradation; and birnessite relies on its substantial Mn(IV) reservoir to maintain long-term oxidative capacity. The absence of detectable •OH and O_2•$^-$ further demonstrates that glyphosate degradation under environmentally relevant conditions proceeds predominantly through mineral-mediated nonradical electron-transfer processes.

Collectively, these findings advance the fundamental understanding of mineral−water interfacial redox chemistry and provide a predictive basis for evaluating glyphosate persistence in soils and sediments containing variable Mn oxide assemblages over pH 3−7. From an applied perspective, the results highlight disordered layered Mn oxides, particularly vernadite, as highly effective and sustainable redox-active materials for glyphosate attenuation. More broadly, the

https://doi.org/10.1021/acs.est.6c00923
Environ. Sci. Technol. 2026, 60, 25686−25700

demonstrated structure-dependent control over degradation pathways underscores the importance of coupling mineralogical context with geochemical conditions when designing Mn-based remediation strategies, particularly when seeking to minimize AMPA accumulation while maximizing glyphosate removal in contaminated environments. In natural waters and soils, coexisting constituents such as dissolved organic carbon and competing oxyanions (e.g., phosphate and silicate) are also expected to influence Mn oxide-glyphosate degradation pathways and mechanisms, particularly at environmentally relevant concentrations. Further investigation of these coupled geochemical effects is therefore needed to achieve a more comprehensive understanding of glyphosate's environmental fate.

■ ASSOCIATED CONTENT

Supporting Information

The Supporting Information is available free of charge at https://pubs.acs.org/doi/10.1021/acs.est.6c00923.

1) Detailed synthesis and characterization of Mn oxides; 2) methods for the quantification of glyphosate and its degradation products and XPS data processing; 3) XRD, Mn, and P K-edge XANES spectra, XPS (Mn 3s, P 2p) spectra, and Mn 2p, O 1s fitting results of samples; 4) UV−vis absorption spectra of Mn(III)-PP formed in the absence of glyphosate and glyphosate degradation kinetics in the presence of PP; 5) HPLC chromatograms of hTPA and TPA after the reaction; 6) mass balance analysis of glyphosate degradation and product formation; degradation rate constants of glyphosate by Mn oxides; 7) speciation distribution of glyphosate and phosphate; 8) ATR-FTIR band assignments for glyphosate adsorption on Mn oxides; 9) potential products of glyphosate degradation by Mn oxides (PDF)

■ AUTHOR INFORMATION

Corresponding Author

Xiaoming Wang − *Key Laboratory of Arable Land Conservation (Middle and Lower Reaches of Yangtze River), Ministry of Agriculture and Rural Affairs, State Environmental Protection Key Laboratory of Soil Health and Green Remediation, Hubei Key Laboratory of Soil Environment and Pollution Remediation, College of Resources and Environment, Huazhong Agricultural University, Wuhan 430070, China;* orcid.org/0000-0002-5484-3922; Email: wangxm338@mail.hzau.edu.cn

Authors

Zhe Liu − *Key Laboratory of Arable Land Conservation (Middle and Lower Reaches of Yangtze River), Ministry of Agriculture and Rural Affairs, State Environmental Protection Key Laboratory of Soil Health and Green Remediation, Hubei Key Laboratory of Soil Environment and Pollution Remediation, College of Resources and Environment, Huazhong Agricultural University, Wuhan 430070, China; School of Environment and Energy, South China University of Technology, Guangzhou 510006, China*

Mengqi Zhang − *Key Laboratory of Arable Land Conservation (Middle and Lower Reaches of Yangtze River), Ministry of Agriculture and Rural Affairs, State Environmental Protection Key Laboratory of Soil Health and Green Remediation, Hubei Key Laboratory of Soil Environment and Pollution Remediation, College of Resources and Environment, Huazhong Agricultural University, Wuhan 430070, China*

Ziyang Zhou − *Key Laboratory of Arable Land Conservation (Middle and Lower Reaches of Yangtze River), Ministry of Agriculture and Rural Affairs, State Environmental Protection Key Laboratory of Soil Health and Green Remediation, Hubei Key Laboratory of Soil Environment and Pollution Remediation, College of Resources and Environment, Huazhong Agricultural University, Wuhan 430070, China*

Xinyu Liu − *Key Laboratory of Arable Land Conservation (Middle and Lower Reaches of Yangtze River), Ministry of Agriculture and Rural Affairs, State Environmental Protection Key Laboratory of Soil Health and Green Remediation, Hubei Key Laboratory of Soil Environment and Pollution Remediation, College of Resources and Environment, Huazhong Agricultural University, Wuhan 430070, China*

Bruno Lanson − *University Grenoble Alpes, CNRS, University Savoie Mont Blanc, IRD, University Gustave Eiffel, ISTerre, Grenoble F-38000, France;* orcid.org/0000-0003-1187-3221

Wantong Zhao − *Key Laboratory of Arable Land Conservation (Middle and Lower Reaches of Yangtze River), Ministry of Agriculture and Rural Affairs, State Environmental Protection Key Laboratory of Soil Health and Green Remediation, Hubei Key Laboratory of Soil Environment and Pollution Remediation, College of Resources and Environment, Huazhong Agricultural University, Wuhan 430070, China*

Xionghan Feng − *Key Laboratory of Arable Land Conservation (Middle and Lower Reaches of Yangtze River), Ministry of Agriculture and Rural Affairs, State Environmental Protection Key Laboratory of Soil Health and Green Remediation, Hubei Key Laboratory of Soil Environment and Pollution Remediation, College of Resources and Environment, Huazhong Agricultural University, Wuhan 430070, China;* orcid.org/0000-0001-5499-7174

Wenfeng Tan − *Key Laboratory of Arable Land Conservation (Middle and Lower Reaches of Yangtze River), Ministry of Agriculture and Rural Affairs, State Environmental Protection Key Laboratory of Soil Health and Green Remediation, Hubei Key Laboratory of Soil Environment and Pollution Remediation, College of Resources and Environment, Huazhong Agricultural University, Wuhan 430070, China*

Guining Lu − *School of Environment and Energy, South China University of Technology, Guangzhou 510006, China*

Complete contact information is available at: https://pubs.acs.org/10.1021/acs.est.6c00923

Notes

The authors declare no competing financial interest.

■ ACKNOWLEDGMENTS

This study was supported by the National Natural Science Foundation of China (No. 42577345), National Key Research and Development Program (No. 2023YFD1702800), the National Modern Agricultural Industry Technology System of China (CARS26), and the Innovative Research Group Project of the Hubei Provincial Natural Science Foundation (2023AFA009). We thank the 4B7A- XAFS Beamline of the Beijing Synchrotron Radiation Facility (https://cstr.cn/31109.

02.BSRF.4B7A) for providing technical support and assistance in XAFS data collection.

REFERENCES

(1) Johal, G. S.; Huber, D. M. Glyphosate effects on diseases of plants. *Eur. J. Agron.* **2009**, *31*, 144−152.

(2) Yaah, V. B. K.; Ahmadi, S.; Quimbayo, M. J.; Morales-Torres, S.; Ojala, S. Recent technologies for glyphosate removal from aqueous environment: a critical review. *Environ. Res.* **2024**, *240*, 117477.

(3) Benbrook, C. M. Trends in glyphosate herbicide use in the United States and globally. *Environ. Sci. Eur.* **2016**, *28*, 3.

(4) Ndjeri, M.; Pensel, A.; Peulon, S.; Haldys, V.; Desmazières, B.; Chaussé, A. Degradation of glyphosate and AMPA (amino methylphosphonic acid) solutions by thin films of birnessite electrodeposited: A new design of material for remediation processes? *Colloids Surf., A* **2013**, *435*, 154−169.

(5) Aparicio, V. C.; De Gerónimo, E.; Marino, D.; Primost, J.; Carriquiriborde, P.; Costa, J. L. Environmental fate of glyphosate and aminomethylphosphonic acid in surface waters and soil of agricultural basins. *Chemosphere* **2013**, *93*, 1866−1873.

(6) Duke, S. O. The history and current status of glyphosate. *Pest Manage. Sci.* **2018**, *74*, 1027−1034.

(7) Ojelade, B. S.; Durowoju, O. S.; Adesoye, P. O.; Gibb, S. W.; Ekosse, G.-I. Review of glyphosate-based herbicide and amino-methylphosphonic acid (AMPA): Environmental and health impacts. *Appl. Sci.* **2022**, *12*, 8789.

(8) Van Bruggen, A. H. C.; He, M. M.; Shin, K.; Mai, V.; Jeong, K. C.; Finckh, M. R.; Morris, J. G. Environmental and health effects of the herbicide glyphosate. *Sci. Total Environ.* **2018**, *616*−*617*, 255−268.

(9) Espinoza-Montero, P. J.; Vega-Verduga, C.; Alulema-Pullupaxi, P.; Fernández, L.; Paz, J. L. Technologies employed in the treatment of water contaminated with glyphosate: A review. *Molecules* **2020**, *25*, 5550.

(10) Sviridov, A. V.; Shushkova, T. V.; Ermakova, I. T.; Ivanova, E. V.; Epiktetov, D. O.; Leontievsky, A. A. Microbial degradation of glyphosate herbicides (Review). *Appl. Biochem. Microbiol.* **2015**, *51*, 188−195.

(11) Grandcoin, A.; Piel, S.; Baurès, E. AminoMethylPhosphonic acid (AMPA) in natural waters: Its sources, behavior and environmental fate. *Water Res.* **2017**, *117*, 187−197.

(12) Paudel, P.; Negusse, A.; Jaisi, D. P. Birnessite-catalyzed degradation of glyphosate: A mechanistic study aided by kinetics batch studies and NMR spectroscopy. *Soil Sci. Soc. Am. J.* **2015**, *79*, 815−825.

(13) Post, J. E. Manganese oxide minerals: Crystal structures and economic and environmental significance. *Proc. Natl. Acad. Sci. U. S. A.* **1999**, *96*, 3447−3454.

(14) Ying, C.; Liu, C.; Zhang, F.; Zheng, L.; Wang, X.; Yin, H.; Tan, W.; Feng, X.; Lanson, B. Solutions for an efficient arsenite oxidation and removal from groundwater containing ferrous iron. *Water Res.* **2023**, *243*, 120345.

(15) Li, F.; Yin, H.; Zhu, T.; Zhuang, W. Understanding the role of manganese oxides in retaining harmful metals: Insights into oxidation and adsorption mechanisms at microstructure level. *Eco-Environ. Health* **2024**, *3*, 89−106.

(16) Li, H.; Fu, B.; Huang, H.; Wu, S.; Ge, J.; Zhang, J.; Li, F.; Qu, P. Catalytic degradation of organic pollutants by manganese oxides: a comprehensive review. *Environ. Pollut. Bioavailab.* **2022**, *34*, 395−406.

(17) Shaikh, N.; Taujale, S.; Zhang, H.; Artyushkova, K.; Ali, A.-M. S.; Cerrato, J. M. Spectroscopic investigation of interfacial interaction of manganese oxide with triclosan, aniline, and phenol. *Environ. Sci. Technol.* **2016**, *50*, 10978−10987.

(18) Song, Y.; Jiang, J.; Ma, J.; Zhou, Y.; von Gunten, U. Enhanced transformation of sulfonamide antibiotics by manganese(IV) oxide in the presence of model humic constituents. *Water Res.* **2019**, *153*, 200−207.

(19) Xiong, R.; Zhang, C.; Xiong, H.; Huang, S.; Li, J. Comparing the abiotic removal of glyphosate by β-MnO2 and δ-MnO2 colloids: Insights into kinetics and mechanisms. *Environ. Pollut.* **2024**, *357*, 124432.

(20) Barrett, K. A.; Mcbride, M. B. Oxidative degradation of glyphosate and aminomethylphosphonate by manganese oxide. *Environ. Sci. Technol.* **2005**, *39*, 9223−9228.

(21) Moller, S. R.; Wallace, A. F.; Zahir, R.; Quadery, A.; Jaisi, D. P. Effect of temperature on the degradation of glyphosate by Mn-oxide: Products and pathways of degradation. *J. Hazard. Mater* **2024**, *461*, 132467.

(22) Azimzadeh, B.; Martínez, C. E. Chemical choreography at the Mn oxide interface: Protein association modulates glyphosate bonding configurations and favors the AMPA oxidation pathway. *Environ. Sci. Technol.* **2025**, *59*, 19513−19525.

(23) Jaisi, D. P.; Li, H.; Wallace, A. F.; Paudel, P.; Sun, M.; Balakrishna, A.; Lerch, R. N. Mechanisms of bond cleavage during manganese oxide and UV degradation of glyphosate: results from phosphate oxygen isotopes and molecular simulations. *J. Agric. Food Chem.* **2016**, *64*, 8474−8482.

(24) Wang, X.; Jones, M. R.; Pan, Z.; Lu, X.; Deng, Y.; Zhu, M.; Wang, Z. Trivalent manganese in dissolved forms: Occurrence, speciation, reactivity and environmental geochemical impact. *Water Res.* **2024**, *263*, 122198.

(25) Newton, A. G.; Kwon, K. D. Classical mechanical simulations of layer- and tunnel-structured manganese oxide minerals. *Geochim. Cosmochim. Acta* **2020**, *291*, 92−109.

(26) Lee, S.; Xu, H.; Xu, W.; Sun, X. The structure and crystal chemistry of vernadite in ferromanganese crusts. *Acta Crystallogr.* **2019**, *75*, 591−598.

(27) Lu, A.; Li, Y.; Ding, H.; Xu, X.; Li, Y.; Ren, G.; Liang, J.; Liu, Y.; Hong, H.; Chen, N.; Chu, S.; Liu, F.; Li, Y.; Wang, H.; Ding, C.; Wang, C.; Lai, Y.; Liu, J.; Dick, J.; Liu, K.; Hochella, M. F. Photoelectric conversion on Earth's surface via widespread Fe- and Mn-mineral coatings. *Proc. Natl. Acad. Sci. U. S. A.* **2019**, *116*, 9741−9746.

(28) Jung, H.; Taillefert, M.; Sun, J.; Wang, Q.; Borkiewicz, O. J.; Liu, P.; Yang, L.; Chen, S.; Chen, H.; Tang, Y. Redox cycling driven transformation of layered manganese oxides to tunnel structures. *J. Am. Chem. Soc.* **2020**, *142*, 2506−2513.

(29) Liang, X.; Post, J. E.; Lanson, B.; Wang, X.; Zhu, M.; Liu, F.; Tan, W.; Feng, X.; Zhu, G.; Zhang, X.; De Yoreo, J. J. Coupled morphological and structural evolution of δ-MnO_2 to α-MnO_2 through multistage oriented assembly processes: the role of Mn(III). *Environ. Sci.: Nano* **2020**, *7*, 238−249.

(30) Liu, H.; Li, Y.; Huangfu, Z.; Lu, Q.; Yang, B.; Liu, Y. Structure and molecular-level transformation for oxidation of effluent organic matters by manganese oxides. *Water Res.* **2024**, *262*, 122082.

(31) McKenzie, R. M. The synthesis of birnessite, cryptomelane, and some other oxides and hydroxides of manganese. *Mineral Mag.* **1971**, *38*, 493−502.

(32) Hinkle, M. A. G.; Flynn, E. D.; Catalano, J. G. Structural response of phyllomanganates to wet aging and aqueous Mn(II). *Geochim. Cosmochim. Acta* **2016**, *192*, 220−234.

(33) Duckworth, O. W.; Sposito, G. Siderophore-manganese(III) interactions II. Manganite dissolution promoted by desferrioxamine B. *Environ. Sci. Technol.* **2005**, *39*, 6045−6051.

(34) Weng, Z.; Rose, M. T.; Tavakkoli, E.; Van Zwieten, L.; Styles, G.; Bennett, W.; Lombi, E. Assessing plant-available glyphosate in contrasting soils by diffusive gradient in thin-films technique (DGT). *Sci. Total Environ.* **2019**, *646*, 735−744.

(35) Li, H.; Wallace, A. F.; Sun, M.; Reardon, P.; Jaisi, D. P. Degradation of glyphosate by Mn-oxide may bypass sarcosine and form glycine directly after C−N bond cleavage. *Environ. Sci. Technol.* **2018**, *52*, 1109−1117.

(36) Li, X.; Yang, P.; Zhao, W.; Guo, F.; Jaisi, D. P.; Mi, S.; Ma, H.; Lin, B.; Feng, X.; Tan, W.; Wang, X. Adsorption mechanisms of glyphosate on ferrihydrite: Effects of Al substitution and aggregation state. *Environ. Sci. Technol.* **2023**, *57*, 14384−14395.

https://doi.org/10.1021/acs.est.6c00923
Environ. Sci. Technol. 2026, 60, 25686−25700

(37) China Standards Press. *GB/T 20684−2017. Glyphosate Water Soluble Powders (Granules)*; China Standards Press: Beijing, China, 2017.
(38) Li, H.; Jaisi, D. P. Competition of sorption and degradation reactions during glyphosate degradation by ferrihydrite/δ-manganese oxide composites. *ACS Earth Space Chem.* **2019**, *3*, 1362−1370.
(39) Liu, W.; Sun, B.; Qiao, J.; Guan, X. Influence of pyrophosphate on the generation of soluble Mn(III) from reactions involving Mn oxides and Mn(VII). *Environ. Sci. Technol.* **2019**, *53*, 10227−10235.
(40) Ying, C.; Lanson, B.; Wang, C.; Wang, X.; Yin, H.; Yan, Y.; Tan, W.; Liu, F.; Feng, X. Highly enhanced oxidation of arsenite at the surface of birnessite in the presence of pyrophosphate and the underlying reaction mechanisms. *Water Res.* **2020**, *187*, 116420.
(41) Zhang, H.; Sui, S.; Zheng, X.; Cao, R.; Zhang, P. One-pot synthesis of atomically dispersed Pt on MnO_2 for efficient catalytic decomposition of toluene at low temperatures. *Appl. Catal., B* **2019**, *257*, 117878.
(42) Wang, Z.; Lv, J.; Zhang, S.; Christie, P.; Zhang, S. Interfacial molecular fractionation on ferrihydrite reduces the photochemical reactivity of dissolved organic matter. *Environ. Sci. Technol.* **2021**, *55*, 1769−1778.
(43) Nesbitt, H. W.; Banerjee, D. Interpretation of XPS Mn(2p) spectra of Mn oxyhydroxides and constraints on the mechanism of MnO_2 precipitation. *Am. Mineral.* **1998**, *83*, 305−315.
(44) Ilton, E. S.; Post, J. E.; Heaney, P. J.; Ling, F. T.; Kerisit, S. N. XPS determination of Mn oxidation states in Mn (hydr)oxides. *Appl. Surf. Sci.* **2016**, *366*, 475−485.
(45) Ravel, B.; Newville, M. ATHENA, ARTEMIS, HEPHAESTUS: data analysis for X-ray absorption spectroscopy using IFEFFIT. *J. Synchrotron Radiat.* **2005**, *12*, 537−541.
(46) Li, F.; Liu, C.; Liang, C.; Li, X.; Zhang, L. The oxidative degradation of 2-mercaptobenzothiazole at the interface of β-MnO_2 and water. *J. Hazard. Mater.* **2008**, *154*, 1098−1105.
(47) Borggaard, O. K.; Gimsing, A. L. Fate of glyphosate in soil and the possibility of leaching to ground and surface waters: a review. *Pest Manage. Sci.* **2008**, *64*, 441−456.
(48) Sidoli, P.; Baran, N.; Angulo-Jaramillo, R. Glyphosate and AMPA adsorption in soils: laboratory experiments and pedotransfer rules. *Environ. Sci. Pollut. Res.* **2016**, *23*, 5733−5742.
(49) Arai, Y.; Sparks, D. L. ATR−FTIR Spectroscopic Investigation on Phosphate Adsorption Mechanisms at the Ferrihydrite−Water Interface. *J. Colloid Interface Sci.* **2001**, *241*, 317−326.
(50) Wang, Q.; Liao, X.; Xu, W.; Ren, Y.; Livi, K. J.; Zhu, M. Synthesis of birnessite in the presence of phosphate, silicate, or sulfate. *Inorg. Chem.* **2016**, *55*, 10248−10258.
(51) Prietzel, J.; Harrington, G.; Häusler, W.; Heister, K.; Werner, F.; Klysubun, W. Reference spectra of important adsorbed organic and inorganic phosphate binding forms for soil P speciation using synchrotron-based K-edge XANES spectroscopy. *J. Synchrotron Radiat.* **2016**, *23*, 532−544.
(52) Liu, Z.; Zhao, W.; Zhang, L.; Wan, B.; Feng, X.; Huang, Q.; Tan, W.; Wang, X. Phytase-mediated hydrolysis of different soil phytate species: Kinetics and mineral interfacial mechanisms. *Geochim. Cosmochim. Acta* **2025**, *403*, 227−239.
(53) Grangeon, S.; Fernandez-Martinez, A.; Claret, F.; Marty, N.; Tournassat, C.; Warmont, F.; Gloter, A. In-situ determination of the kinetics and mechanisms of nickel adsorption by nanocrystalline vernadite. *Chem. Geol.* **2017**, *459*, 24−31.
(54) Zhang, N.; Sun, H.; Zhan, G.; Zu, J.; Zhang, L. Green glyphosate treatment with ferrihydrite and CaO_2 via forming surface ternary complex. *Environ. Sci. Technol.* **2025**, *59*, 2791−2801.
(55) Yang, S.; Shobnam, N.; Sun, Y.; Löffler, F. E.; Im, J. The relative contributions of Mn(III) and Mn(IV) in manganese dioxide polymorphs to bisphenol A degradation. *J. Hazard. Mater.* **2024**, *461*, 132596.
(56) Zhang, S.; Lv, J.; Han, R.; Wang, Z.; Christie, P.; Zhang, S. Sustained production of superoxide radicals by manganese oxides under ambient dark conditions. *Water Res.* **2021**, *196*, 117034.
(57) Wang, Y.; Benkaddour, S.; Marafatto, F. F.; Peña, J. Diffusion- and pH-dependent reactivity of layer-type MnO_2: reactions at particle edges versus vacancy sites. *Environ. Sci. Technol.* **2018**, *52*, 3476−3485.
(58) Zhao, H.; Zhu, M.; Li, W.; Elzinga, E. J.; Villalobos, M.; Liu, F.; Zhang, J.; Feng, X.; Sparks, D. L. Redox reactions between Mn(II) and hexagonal birnessite change its layer symmetry. *Environ. Sci. Technol.* **2016**, *50*, 1750−1758.
(59) Yang, P.; Post, J. E.; Wang, Q.; Xu, W.; Geiss, R.; McCurdy, P. R.; Zhu, M. Metal adsorption controls stability of layered manganese oxides. *Environ. Sci. Technol.* **2019**, *53*, 7453−7462.
(60) Wang, Q.; Yang, P.; Zhu, M. Structural transformation of birnessite by fulvic acid under anoxic conditions. *Environ. Sci. Technol.* **2018**, *52*, 1844−1853.
(61) Wang, Z.; Shi, Z.; Xu, T.; Zhu, Y.; Zhao, H.; Xie, W.; Qi, B.; Zhang, C.; Zhu, K.; Jia, H. MnO_2 structural polymorph-mediated interaction with dissolved organic matter: underlying protection and transformation mechanisms. *Environ. Sci. Technol.* **2025**, *59*, 26583−26592.
(62) Wang, L.; Jiang, J.; Pang, S.-Y.; Zhou, Y.; Li, J.; Sun, S.; Gao, Y.; Jiang, C. Oxidation of bisphenol A by nonradical activation of peroxymonosulfate in the presence of amorphous manganese dioxide. *Chem. Eng. J.* **2018**, *352*, 1004−1013.
(63) Zhang, H.; Chen, W.-R.; Huang, C.-H. Kinetic modeling of oxidation of antibacterial agents by manganese oxide. *Environ. Sci. Technol.* **2008**, *42*, 5548−5554.
(64) Chen, D.; Zhao, R.; Liu, H.; Tian, Y.; Deng, C.; Chen, C.; Liu, X.; Huang, D.; Huang, Y. Selective glyphosate degradation via oxygen activation using Fe-N-C: Critical role of size exclusion. *J. Hazard. Mater.* **2025**, *490*, 137810.
(65) Saputra, E.; Muhammad, S.; Sun, H.; Ang, H. M.; Tadé, M. O.; Wang, S. Different crystallographic one-dimensional MnO_2 nanomaterials and their superior performance in catalytic phenol degradation. *Environ. Sci. Technol.* **2013**, *47*, 5882−5887.
(66) He, C.; Wang, Y.; Li, Z.; Huang, Y.; Liao, Y.; Xia, D.; Lee, S. Facet engineered α-MnO_2 for efficient catalytic ozonation of odor CH_3SH: Oxygen vacancy-induced active centers and catalytic mechanism. *Environ. Sci. Technol.* **2020**, *54*, 12771−12783.

Supplementary Information

Structure-Dependent Oxidation Mechanisms of Glyphosate by Manganese Oxides: Role of Mineralogy and pH

Zhe Liu[a,b], Mengqi Zhang[a], Ziyang Zhou[a], Xinyu Liu[a], Bruno Lanson[c], Wantong Zhao[a], Xionghan Feng[a], Wenfeng Tan[a], Guining Lu[b], Xiaoming Wang[a*]

[a] Key Laboratory of Arable Land Conservation (Middle and Lower Reaches of Yangtze River), Ministry of Agriculture and Rural Affairs, State Environmental Protection Key Laboratory of Soil Health and Green Remediation, College of Resources and Environment, Huazhong Agricultural University, Wuhan 430070, China

[b] School of Environment and Energy, South China University of Technology, Guangzhou 510006, China

[c] Univ. Grenoble Alpes, Univ. Savoie-Mont Blanc, CNRS, IRD, IFSTTAR, ISTerre, F-38000 Grenoble, France

*Corresponding author:

Xiaoming Wang, E-mail: wangxm338@mail.hzau.edu.cn

Number of pages: 16

Number of texts: 3

Number of figures: 12

Number of tables: 4

Text S1: Preparation and characterization of Mn oxides

Synthesis of Mn Oxides: To synthesize K-birnessite, 300 mL of 0.667 M $KMnO_4$ was prepared and boiled in a thermostatic oil bath at 110 °C, 45 mL of 6 M HCl was added at a rate of 0.7 mL/min while stirring. The mixture was kept boiling for 30 min and aged at 60 °C for 16 h.[1] To synthesize vernadite, 750 mL of 0.15 M $Mn(NO_3)_2$ was gradually added at a rate of 10 mL/min into a mixture containing 750 mL of 0.1 M $KMnO_4$ and 0.2 M NaOH while stirring. The suspension was then aged at room temperature for 20 h.[2] For the synthesis of cryptomelane, 8.45 g of $MnSO_4 \cdot 4H_2O$ was dissolved in 100 mL of 2 M acetic acid solution. Simultaneously, an 80 mL solution of 0.44 M $KMnO_4$ was prepared. Two solutions were heated to 60 °C and mixed by continuous stirring. The mixture was further heated to 100 °C for 20 min before cooling to 60 °C for 24 h of aging.[1] The synthesis of manganite was modified by the method of Duckworth and Sposito.[3] A mixture of 100 mL of 1.4 M $MnSO_4 \cdot H_2O$ and 100 mL of 0.4 M $NH_3 \cdot H_2O$ was prepared. Then, 90 mL of H_2O_2 solution was added at a rate of 3 mL/min. After the addition, the suspension was placed in an oil bath at 105 °C under reflux for 24 h. All these obtained Mn oxides were washed using deionized water, freeze-dried, ground, and labeled as birnessite, vernadite, crytomelane, and manganite, respectively.

X-ray Diffraction: Mn oxides were characterized using a Bruker D8 ADVANCE X-ray diffractometer (XRD) with Cu Kα radiation (λ = 0.15418 nm), an operating voltage of 40 kV, and a current of 40 mA. The scanning range was 5-85°, with a speed of 1°/min and a step size of 0.02°.

Elemental Composition: 0.1000 g of each sample was accurately weighed into a conical

flask, followed by the addition of 25 mL of 0.25 M hydroxylamine hydrochloride. Then, 1 M H_2SO_4 was added to dissolve the sample completely. After dissolution, the solution was transferred to a 250 mL volumetric flask and brought to volume with deionized water, followed by thorough mixing. Metal concentrations were measured using a flame atomic absorption spectrometer (Varian AAS240FS), and Na^+/K^+ contents were determined using a flame photometer (Sherwood Model 410).

Mn K-edge XAS: Mn K-edge X-ray absorption spectroscopy (XAS) was performed at the 1W1B beamline of the Beijing Synchrotron Radiation Facility (BSRF) in transmission mode using a Si(111) double-crystal monochromator. The energy resolution was $1–3 \times 10^{-4}$. The electron beam energy was 2.5 GeV with a maximum beam current of 250 mA. Spectral background subtraction and fitting analyses were performed using Athena software.

Specific Surface Area and Pore Structure: Birnessite, vernadite, and cryptomelane were degassed at 100 °C, 60 °C, and 120 °C for 6 h, 12 h, and 6 h, respectively, to remove adsorbed water and volatiles prior to specific surface area (SSA) and pore size distribution measurements. N_2 adsorption-desorption isotherms were obtained using an automatic surface area and porosity analyzer (Micromeritics ASAP 2460), and the five-point Brunauer-Emmett-Teller (BET) and the Discrete Fourier Transform (DFT) method were employed for the calculations.

Zeta Potential Measurements: The Zeta potential of the Mn oxides suspension was measured using a Malvern Zetasizer Nano ZS. Suspensions were prepared at a mineral concentration of 0.2 g/L in 0.01 M NaCl background solution, and the pH was adjusted over the range 1-8 using 0.01-1 M NaOH or HCl. Each measurement was conducted in triplicate,

and the average value was reported.

Redox Potential Measurements: The redox potential of the Mn oxides suspensions was determined by an automatic potentiometric titrator (Metrohm 907) equipped with a platinum electrode as the working indicator electrode and an Ag/AgCl electrode as the reference electrode. The mineral concentration was maintained at 0.2 g/L, and the pH range was adjusted in the range 3-10 using 0.01-1 M NaOH or HCl. Measurements were performed at room temperature, and each sample was measured three times to ensure reproducibility, with the mean values reported.

Text S2: Determination of glyphosate and its degradation products

1 mL of the filtrate of degradation product was mixed with 0.12 mL of 5% boric acid buffer, adjusting the pH to 9. Then, 0.12 mL of 12,000 mg/L 9-fluorenylmethyl chloroformate (FMOC) in acetonitrile (ACN) solution was added, and derivatization was carried out at 22 ± 1 °C for 16 h. The reaction was terminated by adding 0.015 mL of 6 M HCl, adjusting the pH to 1.5. After 1 h, the derivatized sample was filtered through a 0.22 μm membrane and analyzed using an Acclaim 120 C18 column (2.1 × 250 mm) with gradient elution. The elution solvent consisted of 5 mM HAc/NH_4Ac (pH 4.8) and acetonitrile. The acetonitrile percentage changed as follows: 5% to 75% from 0 to 42 min, 100% from 42.1 to 45 min, and 5% from 45.1 to 55 min. All samples were completely separated within 55 min.[4]

Glyphosate concentrations were determined spectrophotometrically based on the formation of N-nitrosoglyphosate through reaction with sodium nitrite under acidic conditions.

Absorbance was recorded at 242 nm, and concentrations were quantified using an external calibration curve.[5]

Text S3: XPS Data Processing

Background subtraction was performed using the Smart-type method. Charge correction was performed by setting the adventitious C 1s peak to 284.8 eV. The average Mn oxidation state (AOS) was determined from the multiplet splitting of the Mn 3s spectra.[6] Overlapping peaks in the Mn $2p_{3/2}$ spectra were deconvoluted using fixed binding energies for Mn(II), Mn(III), and Mn(IV), with equal full width at half maximum (FWHM) for all components. The quantified Mn species are subject to inherent uncertainty associated with spectral resolution, background selection, and peak deconvolution.[7] For O 1s spectra, the FWHM of all peaks was kept constant. Peak fitting employed incorporating Lorentzian/ Gaussian line shape.[8]

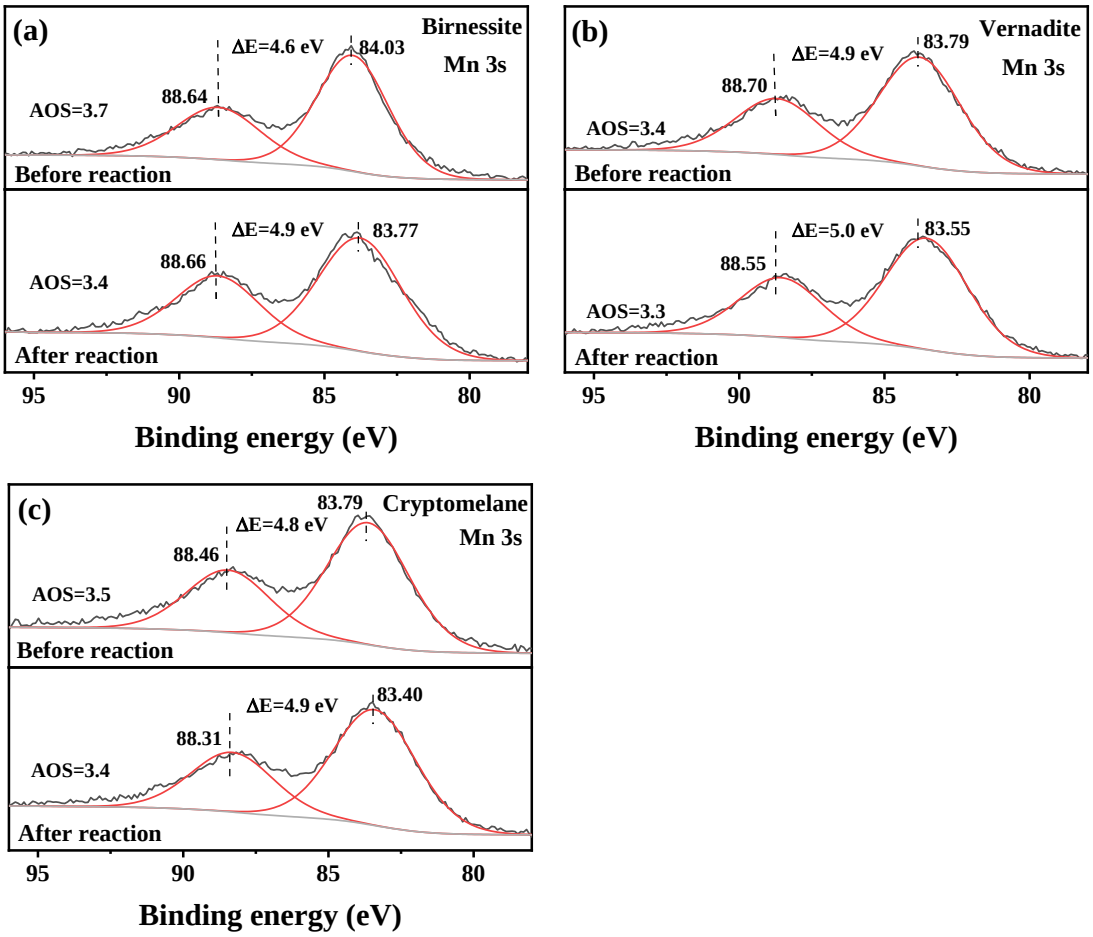

Figure S1. XPS Mn 3s spectra of Mn oxides before and after glyphosate degradation: (a) birnessite, (b) vernadite, and (c) cryptomelane. Binding energies were charge-corrected using the adventitious C 1s peak at 284.8 eV. Reaction conditions: 0.5 g/L Mn oxides, 100 mg/L glyphosate, 0.01 mol/L NaCl as the background electrolyte, and pH 7 ± 0.1.

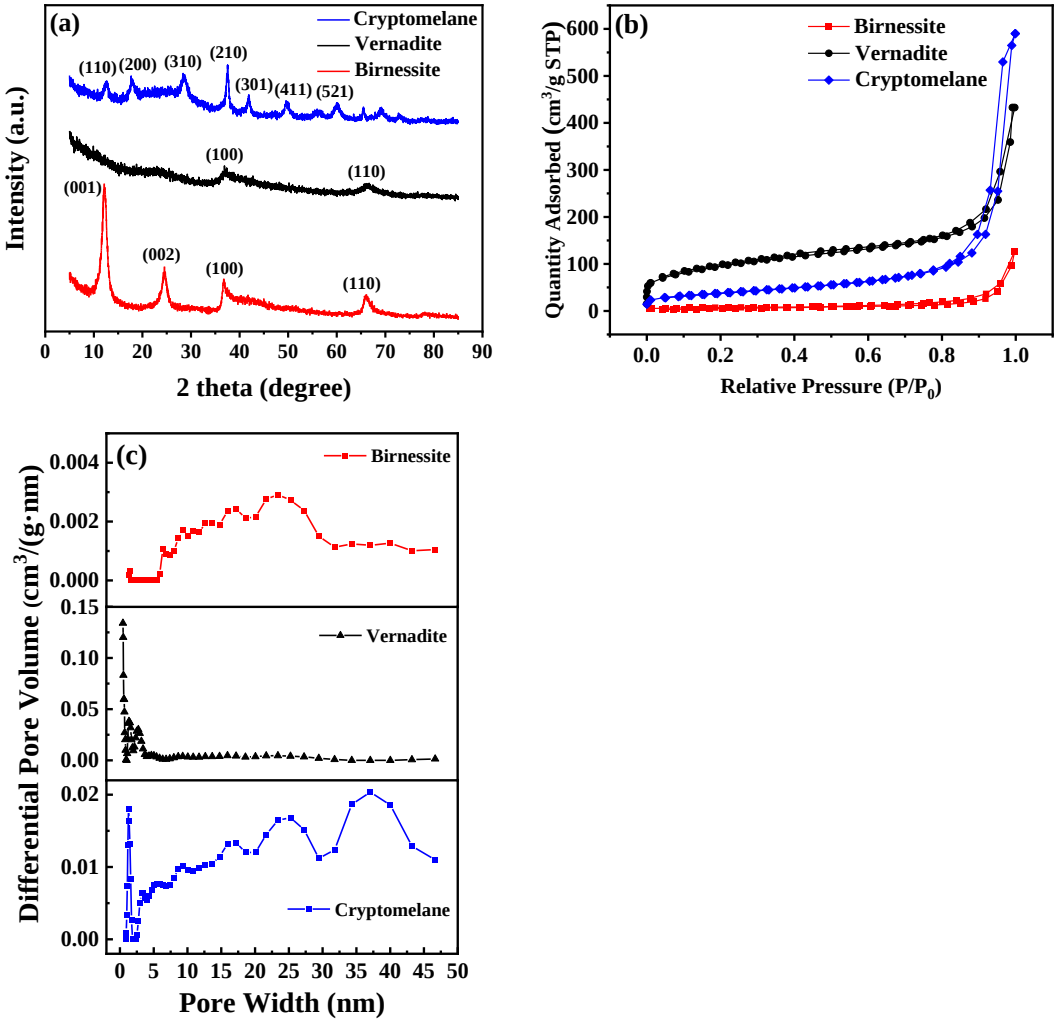

Figure S2. Physicochemical characterization of the synthesized Mn oxides: XRD patterns (a), N_2 adsorption-desorption isotherms (b), and pore size distribution curves calculated by density functional theory (c).

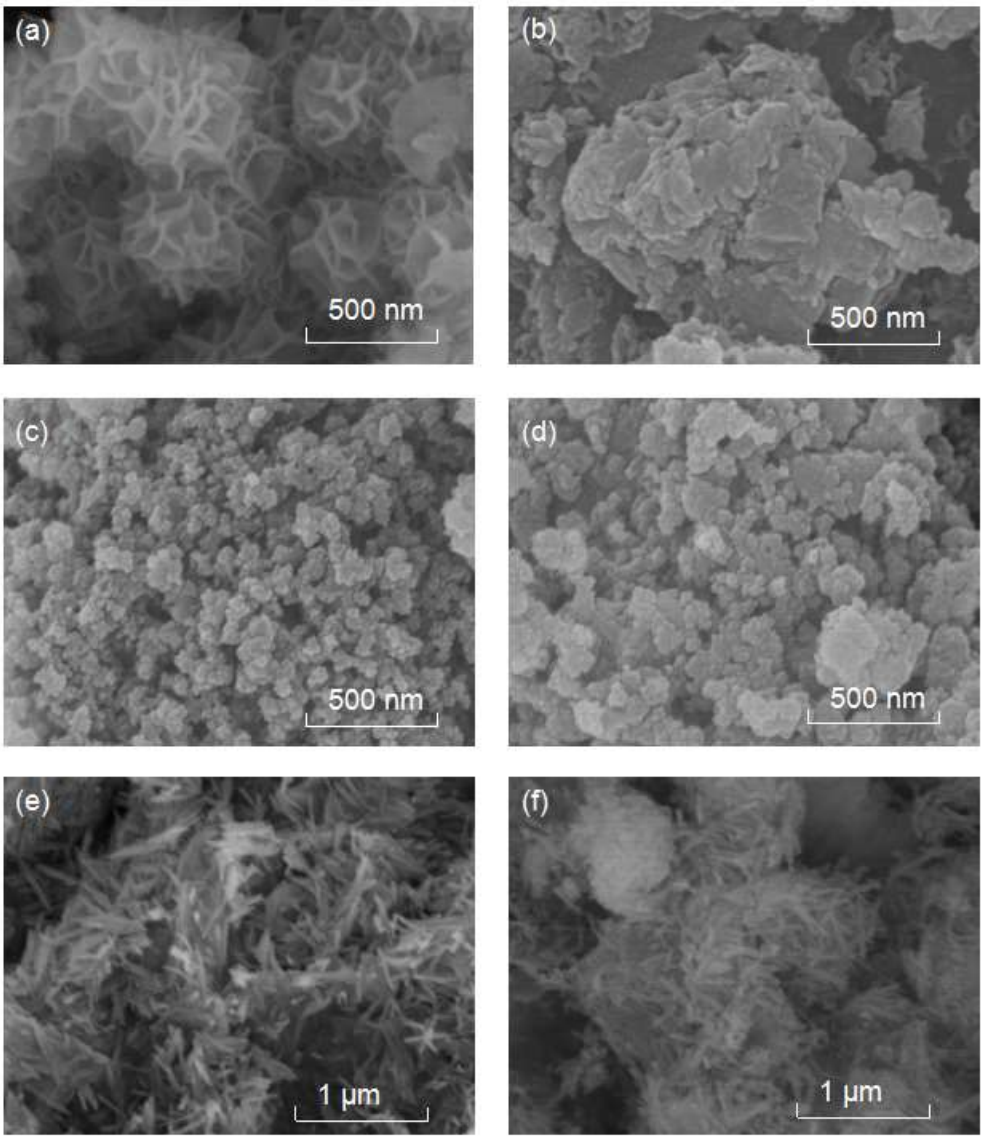

111

112 **Figure S3.** SEM images of Mn oxides before (a: birnessite; c: vernadite; e: cryptomelane) and
113 after (b: birnessite; d: vernadite; f: cryptomelane) glyphosate degradation. The Mn oxide
114 loading was 0.5 g/L, the initial concentration of glyphosate was 100 mg/L, pH was 7 ± 0.1, and
115 the reaction was in dark at room temperature for 24 h.

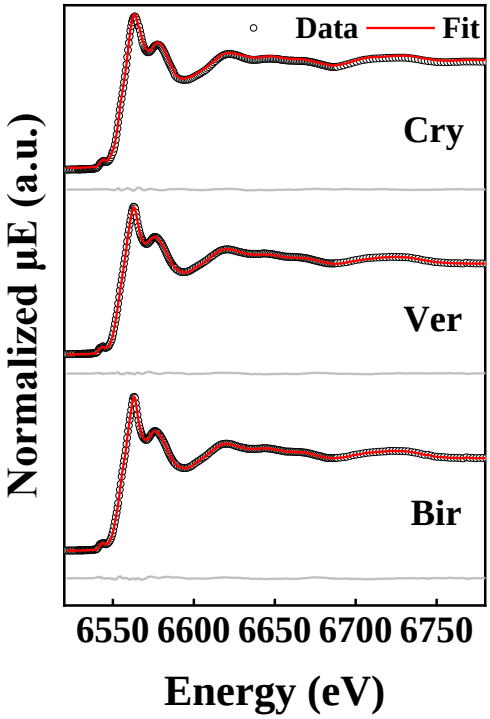

Figure S4. Mn K-edge XANES spectra of Mn oxides and fitting using the Combo method.

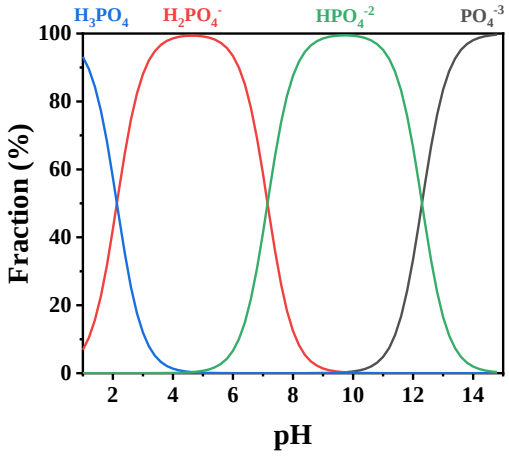

Figure S5. The speciation diagram of phosphate.

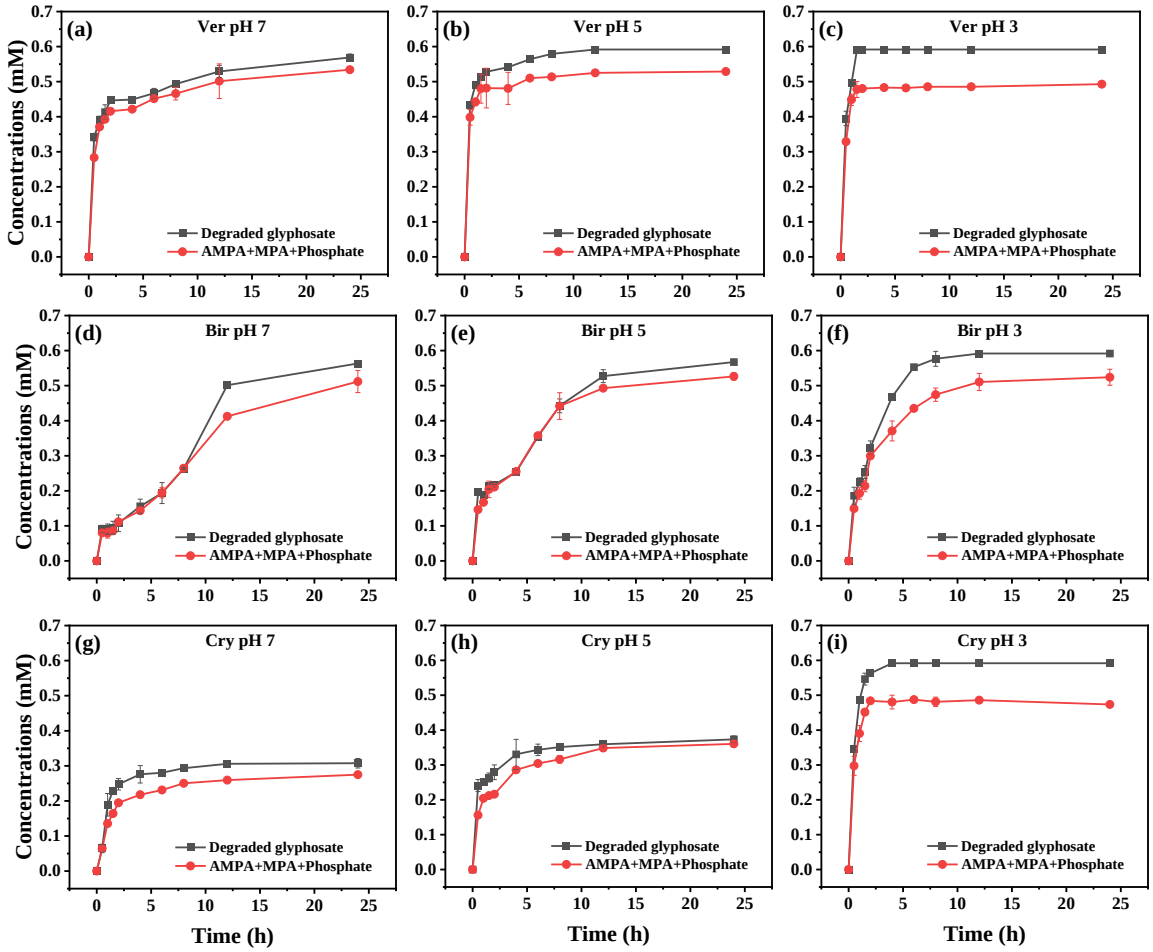

Figure S6. Mass balance analysis of glyphosate degradation and product formation (AMPA, methylphosphonic acid (MPA), phosphate) during Mn oxide-mediated oxidation, for vernadite (a–c), birnessite (d–f), and cryptomelane (g–i) at pH 3, 5, and 7. Experiments were conducted with an initial glyphosate concentration of 100 mg/L and a Mn oxide loading of 0.5 g/L. Note: The concentration of MPA was estimated from the molar amount of glycine, assuming equimolar formation of glycine and MPA via C(3)–N bond cleavage of glyphosate. Both glycine and MPA are considered resistant to further oxidation by Mn oxides under the experimental conditions.[9]

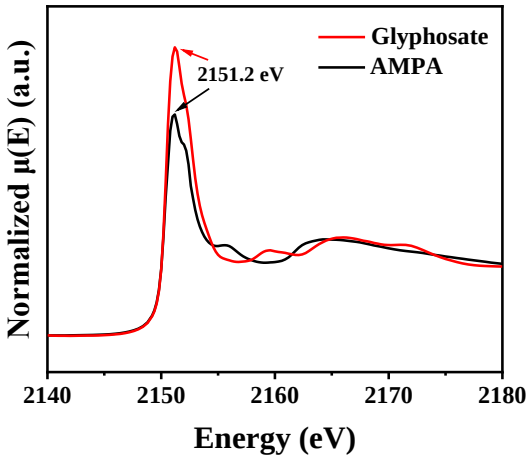

135

136 **Figure S7.** P K-edge X-ray absorption near edge structure (XANES) spectra for pure
137 glyphosate and AMPA. Pure glyphosate and AMPA powders were diluted with boron nitride
138 (BN) to achieve 15,000–20,000 mg P/kg prior to XANES measurements.

139

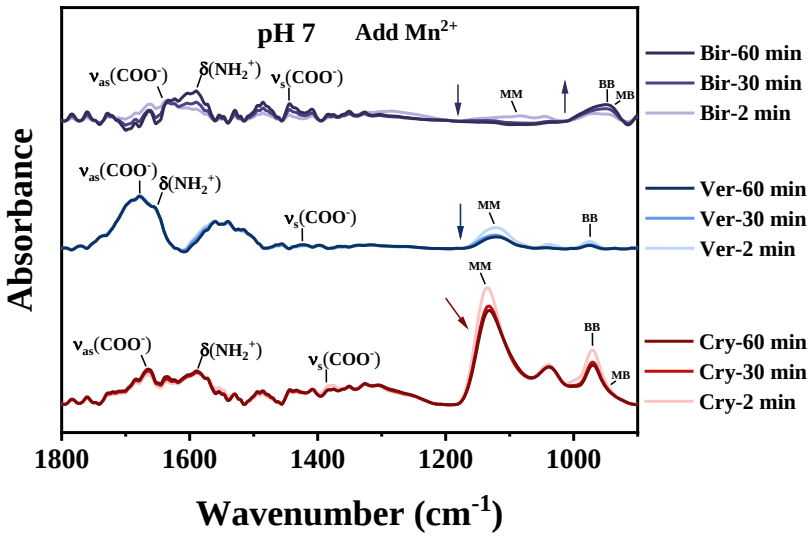

140

141 **Figure S8.** Figure S9. ATR-FTIR spectra of glyphosate adsorption-oxidation on Mn oxide
142 surfaces at pH 7 over 60 min, followed by continuous flow of a 10 mg/L Mn(II) solution. The
143 indicated times represent the elapsed time after the start of Mn(II) flow.

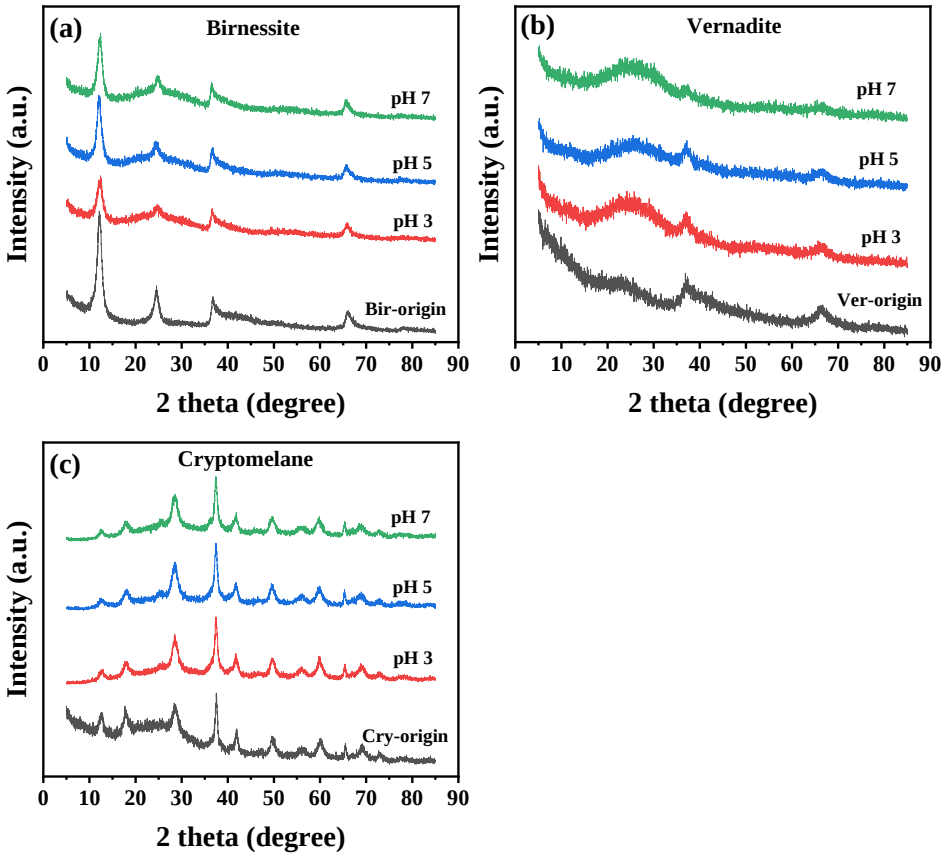

Figure S9. XRD patterns of Mn oxides before and after glyphosate degradation. Reaction conditions: 0.5 g/L Mn oxides, 100 mg/L glyphosate, 0.01 mol/L NaCl, and pH 7 ± 0.1, a: birnessite; b: vernadite; c: cryptomelane.

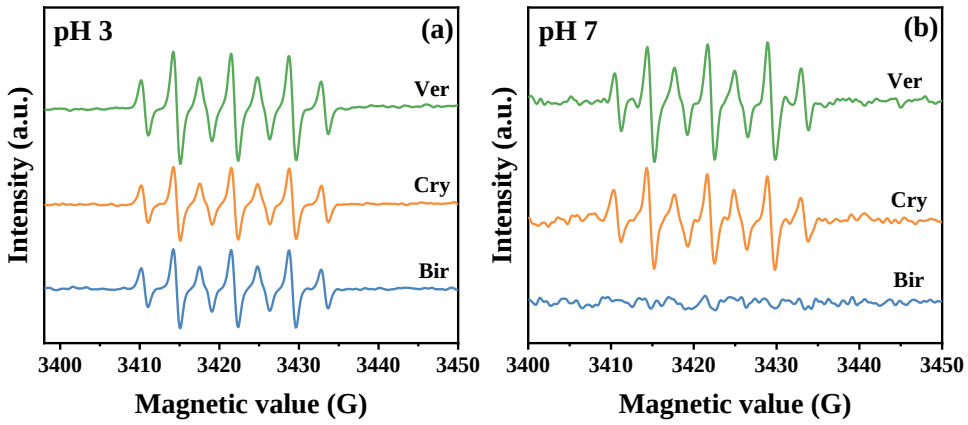

Figure S10. EPR spectra of Mn oxides (0.2 g/L) with DMPO as a spin-trapping agent at pH 3.0 (a) and pH 7.0 (b). Cry: cryptomelane; Ver: vernadite; Bir: birnessite.

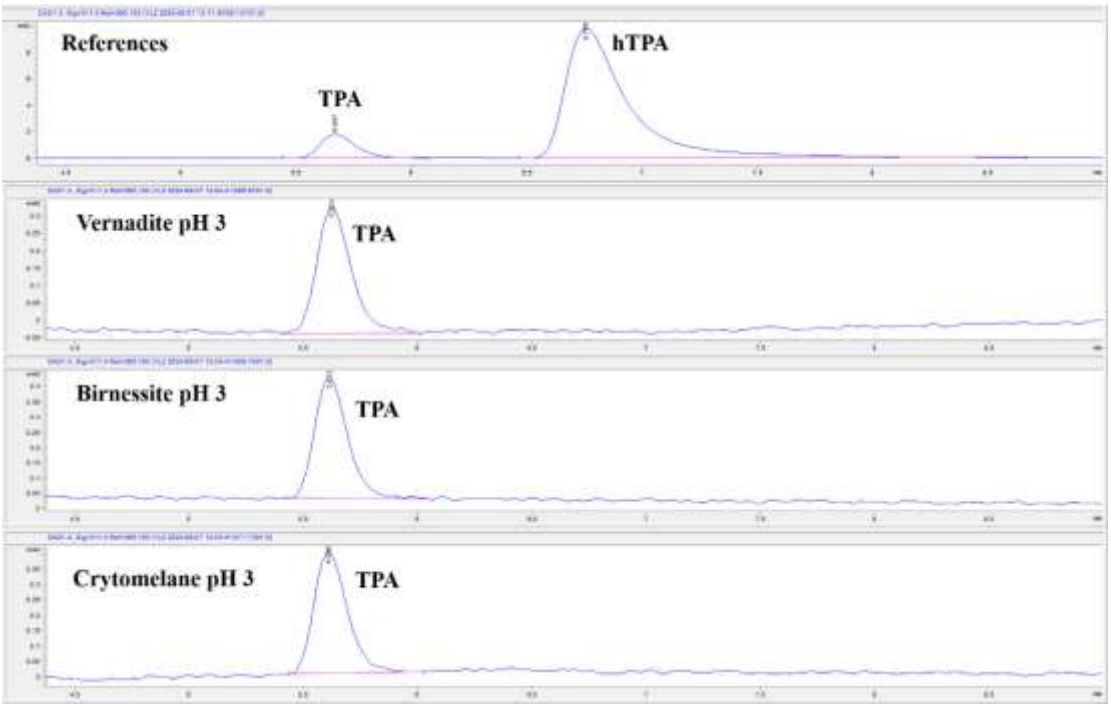

Figure S11. HPLC chromatograms of hTPA and TPA after the reaction between 0.2 mM TPA and Mn oxides for 24 h at pH 3.

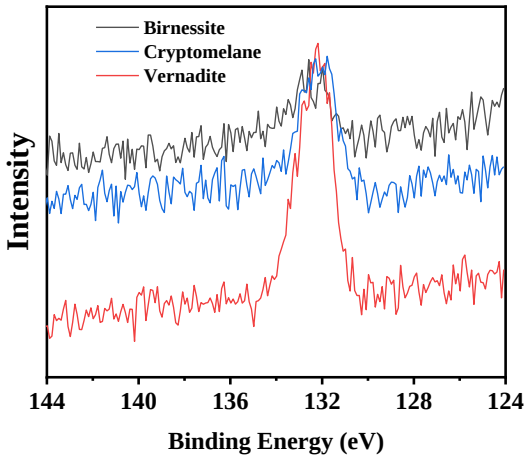

Figure S12. XPS P 2p spectra of solid products from glyphosate degradation by Mn oxides. Reaction conditions: 0.5 g/L Mn oxides, 100 mg/L glyphosate, 0.01 mol/L NaCl, and pH 7 ± 0.1.

163 **Table S1.** Fitting results of Mn K-edge XANES spectra of Mn oxides using the Combo method

Samples	Mn(II) (%)	Mn(III) (%)	Mn(IV) (%)	R-factor	Mn AOS
Birnessite	1.50	5.80	92.70	0.00005	3.91
Vernadite	1.00	11.50	87.50	0.00003	3.88
Cryptomelane	1.17	14.17	84.67	0.00002	3.83

164

165 **Table S2.** Degradation kinetic constants (k) of glyphosate by Mn oxides

	pH	k (min^{-1})	R^2
Birnessite	7	0.0007	0.8706
	5	0.0013	0.9091
	3	0.0033	0.9698
Vernadite	7	0.0150	0.9763
	5	0.0152	0.9735
	3	0.0176	0.9785
Crytomelane	7	0.0028	0.8599
	5	0.0039	0.9340
	3	0.0065	0.9528

166

167 **Table S3.** Possible assignments of characteristic infrared bands for glyphosate adsorption on
168 Mn oxide surfaces. MM, BB, and MB denote monodentate mononuclear, bidentate binuclear,
169 and mononuclear bidentate complexes, respectively.

Assignments	Wavenumber (cm^{-1})					
	Birnessite		Vernadite		Cryptomelane	
	pH 5	pH 7	pH 5	pH 7	pH 5	pH 7
$\nu_{as}(COO^-)$	1604	1639	1679	1678	1641	1666
$\delta(NH_2^+)$	1589	1627	1645	1654	1573	1589
$\nu_s(COO^-)$	1444	1407	1396	1400	1392	1377
$\nu(POMn)_{MM}$	1093	1101	1116	1120	1136	1136
$\nu(P(OMn)_2)_{BB}$	975	972	979	975	974	970
$\nu(P(O)_2Mn)_{MB}$	954	947	925	923	929	931

Table S4. Potential products of glyphosate degradation by Mn oxides

Pathways	By-products	Molecular structure	Molecular weight
/	Glyphosate		169
Pathway 2	AMPA		111
Pathway 3	Glycine	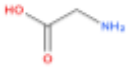	75
Pathway 3	Methylphosphonic acid[9]		96
Pathway 3	Formaldehyde[9]		30
Pathway 2/3	Phosphate	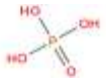	98
Pathway 2/3	Formic acid[11]		46
Pathway 2/3	Nitrate ion[12]		62
Pathway 2/3	Ammonium ion[12]		18
Pathway 2/3	Carbon dioxide[12]		44

References

1. McKenzie, R. M. The synthesis of birnessite, cryptomelane, and some other oxides and hydroxides of manganese. *Mineral. Mag.* **1971,** *38*, 493-502.

2. Hinkle, M. A. G.; Flynn, E. D.; Catalano, J. G. Structural response of phyllomanganates to wet aging and aqueous Mn(II). *Geochim. Cosmochim. Acta* **2016,** *192*, 220-234.

3. Duckworth, O. W.; Sposito, G. Siderophore-manganese(III) interactions II. manganite dissolution promoted by desferrioxamine B. *Environ. Sci. Technol.* **2005,** *39*, 6045-6051.

4. Li, H.; Jaisi, D. P. Competition of sorption and degradation reactions during glyphosate degradation by ferrihydrite/δ-manganese oxide composites. *ACS Earth Space Chem.* **2019,** *3*, 1362-1370.

5. *GB/T 20684-2017. Glyphosate Water Soluble Powders (Granules)*; China Standards Press: Beijing, China, **2017**.

6. Ilton, E. S.; Post, J. E.; Heaney, P. J.; Ling, F. T.; Kerisit, S. N. XPS determination of Mn oxidation states in Mn (hydr)oxides. *Appl. Surf. Sci.* **2016,** *366*, 475-485.

7. Biesinger, M. C.; Payne, B. P.; Grosvenor, A. P.; Lau, L. W. M.; Gerson, A. R.; Smart, R. S. C. Resolving surface chemical states in XPS analysis of first row transition metals, oxides and hydroxides: Cr, Mn, Fe, Co and Ni. *Appl. Surf. Sci.* **2011,** *257*, 2717-2730.

8. Nesbitt, H. W.; Banerjee, D. Interpretation of XPS Mn(2p) spectra of Mn oxyhydroxides and constraints on the mechanism of MnO_2 precipitation. *Am. Mineral.* **1998,** *83*, 305–315.

9. Li, H.; Wallace, A. F.; Sun, M.; Reardon, P.; Jaisi, D. P. Degradation of glyphosate by Mn-oxide may

bypass sarcosine and form glycine directly after C–N bond cleavage. *Environ. Sci. Technol.* **2018,** *52*, 1109-1117.

10. He, C.; Wang, Y.; Li, Z.; Huang, Y.; Liao, Y.; Xia, D.; Lee, S. Facet engineered α-MnO_2 for efficient catalytic ozonation of odor CH_3SH: Oxygen vacancy-induced active centers and catalytic mechanism. *Environ. Sci. Technol.* **2020,** *54*, 12771-12783.

11. Paudel, P.; Negusse, A.; Jaisi, D. P. Birnessite-catalyzed degradation of glyphosate: A mechanistic study aided by kinetics batch studies and NMR spectroscopy. *Soil Sci. Soc. Am. J.* **2015,** *79*, 815-825.

12. Ndjeri, M.; Pensel, A.; Peulon, S.; Haldys, V.; Desmazières, B.; Chaussé, A. Degradation of glyphosate and AMPA (amino methylphosphonic acid) solutions by thin films of birnessite electrodeposited: A new design of material for remediation processes? *Colloids Surf. A Physicochem. Eng. Asp.* **2013,** *435*, 154-169.